Surface Science Reports 73 (2018) 213–232

Contents lists available at ScienceDirect

Surface Science Reports

journal homepage: www.elsevier.com/locate/surfrep

Pauling's rules for oxide surfaces

Tassie K. Andersen [a, *], Dillon D. Fong [b], Laurence D. Marks [a]

[a] Department of Materials Science and Engineering, Northwestern University, Evanston, IL 60208, United States
[b] Materials Science Division, Argonne National Laboratory, Argonne, IL 60439, United States

ARTICLE INFO

Article history:
Received 29 May 2018
Received in revised form
7 August 2018
Accepted 17 August 2018
Available online 12 September 2018

Keywords:
Oxide surfaces
Surface structure
Perovskite oxides
Surface reconstructions
Reconstructions
Strontium titanate

ABSTRACT

Determination of surface structures currently requires careful measurement and computationally expensive methods since, unlike bulk crystals, guiding principles for generating surface structural hypotheses are frequently lacking. Herein, we discuss the applicability of Pauling's rules as a set of guidelines for surface structures. The wealth of solved reconstructions on $SrTiO_3$ (100), (110), and (111) are considered, as well as nanostructures on these surfaces and a few other ABO_3 oxide materials. These rules are found to explain atomic arrangements for reconstructions and thin films just as they apply to bulk oxide materials. Using this data and Pauling's rules, the fundamental structural units of reconstructions and their arrangement are discussed.

Contents

1. Introduction

Oxide surfaces are an important frontier, with applications in areas ranging from catalysis to the emerging field of oxide electronics [1–8]. Our understanding of oxide surfaces is relatively primitive and it is often mistakenly assumed that they are simple bulk truncations. There is a large body of evidence indicating that many oxide surfaces reconstruct to form large complex unit cells that make the reconstructions found on elemental metals or semiconductors look simple. For instance, the archetypal perovskite $SrTiO_3$ has more reconstructions than silicon. Some of them, e.g. the $(n \times n)$ family on the (111) surface with $(2 < n < 6)$ [9–11], are more complicated than the Si (111) (7×7) reconstruction [12–14]. These reconstructions form under a diverse set of

* Corresponding author.
E-mail address: tassie_andersen@amat.com (T.K. Andersen).

https://doi.org/10.1016/j.surfrep.2018.08.001
0167-5729/

Abbreviations

LEED	Low-energy electron diffraction
STM	Scanning tunneling microscopy
DFT	Density functional theory
TED	Transmission electron diffraction
SXRD	Surface X-ray diffraction
BVS	Bond valence sum
ED-TiO_4	Edge-displaying TiO_4
FD-TiO_4	Face-displaying TiO_4

conditions including single crystals annealed in oxygen or vacuum, thin films grown by hybrid molecular beam epitaxy, and during hydrothermal synthesis of nanoparticles [5,15–21]. Few atomic structures of these reconstructions are known, due to experimental complications in reproducing them and because the workhorses of structure determination for conductors (low energy electron diffraction (LEED) and scanning tunneling microscopy (STM)) are less effective for insulators. Even when insulators can be doped, STM is useful but can have limited spatial resolution. Going beyond $SrTiO_3$ to more complex perovskites such as $KTaO_3$, $NdGaO_3$, $LaAlO_3$ or $DyScO_3$, there is almost no information about the thermodynamically stable surface structures. Despite this, the number of publications where oxides films have been grown on perovskite substrates is rapidly increasing [22–25]. Rarely acknowledged in the open literature (but known in the unspoken literature), growth is often experimentally irreproducible, and we hypothesize that in many cases this is due to uncontrolled initial surface structures.

If we do not know the positions of the atoms at the surface, it is impossible to explain phenomena that change depending on the surface reconstruction such as the different shapes and catalytic behavior of nanoparticles [26–34], different growth modes of technologically important materials, and different surface chemical reactivity [35–40], as well as the unspoken irreproducibility of many oxide growth experiments. Additionally, the understanding of properties suffers for those that rely on controlled interfaces and surfaces such as superconductivity [41,42] and magneto-electric coupling [43].

The process of solving a surface structure often depends on multiple experimental and theoretical techniques with varying levels of complexity for quantitative analysis. Often, simpler experimental techniques require more involved analysis and some common methods will be discussed briefly in the order from most- to least-demanding evaluation. Reconstructions can be experimentally identified with reflection high-energy electron diffraction or LEED data. This data, with the proper analysis, can be used to solve a surface structure provided it is not too complex [44,45]. STM probes the local density of states and atom heights, revealing information regarding the position of atoms at the surface and is a method for identifying reconstructions and their basic structural features [46–48]. Density functional theory (DFT) can be used to relax hypothetical surface structures and supplement experimental results to improve understanding [49,50]. DFT can also be used to calculate energetic stability as a function of chemical potential, allowing for comparison between structures synthesized differently. Pairing STM with DFT calculations allows low-energy solutions to be identified and the electron density from DFT can be used to simulate STM. More straightforward information can be obtained from transmission electron diffraction (TED) [51] or surface x-ray diffraction (SXRD) [52,53], which can be combined with direct methods [54,55] to unambiguously determine the positions of many atoms in a reconstruction. Additionally, atomic positions from DFT can be used to produce simulated diffraction patterns by calculating the resulting structure factor, providing one more method for verification.

The simple binary oxides have only limited degrees of freedom, so their surfaces are relatively easy to understand. Beyond them, one of the most common structures is the perovskite, ABO_3, which can be described as alternating layers of AO and BO_2 oxygen-coordinated cations in the [001] direction. Many perovskites have both a transition metal as their B-site cation, where the transition metals have correlated electrons that display unique properties based on their electron interactions, and similar structures and lattice parameters [25,56]. Combinations of the methods described above have furnished structure solutions of perovskite oxide surfaces, particularly for $SrTiO_3$ [9–11,15,20,47,48,57–82]. The (100), (110), and (111) surfaces have all been studied, and are representative of the challenges - they are insulating, two are polar, and one possesses a mixed A/B cation termination when truncated along an idealized atomic plane. Other oxides with published reconstructions include $BaTiO_3$ [83–87], $LaAlO_3$ [88], $LiNbO_3$ [89], and $PbTiO_3$ [90], although the number of reconstructions solved on these surfaces is far fewer.

While experimental methods and simulation have been applied to the problem of solving reconstructions, the theoretical framework for understanding and predicting these structures is incomplete. One can approach this problem from two directions: the first is general formulations based upon the underlying physics/chemistry, and the second is specific calculations typically using density functional schemes. Explanations using the first approach include concepts such as surface dangling bonds [91] or minimizing Coulomb forces [92]. In the case of oxides with polar surfaces, issues such as charge compensation [93,94] serve to further complicate this picture. In all of these the fundamental idea is that a surface must be valence-neutral and not contain an unbalanced electrostatic dipole. (We will return to this later, discussing more some of subtleties of the terms “valence” and “charge”.)

In the second approach, based upon *ab initio* calculations, oxide surfaces are often described as ideal truncations of the bulk crystal. This fails to capture the nuance of perovskites and the variety of reconstructions that have been observed on their surfaces [62,66,83,89,95]. Oversimplifying surfaces by representing them as bulk truncations, even with oxygen vacancies, is poor science in many cases and does not agree with experimental evidence. In addition, while *ab initio* methods have had notable successes, they are not guaranteed to produce the correct result. By their nature, most such methods will relax atomic positions into a local energy minimum. If the initial positions of atoms in a hypothetical structure model are too far from the true structure, the end result may represent a local rather than global energy minimum – i.e. the structure is wrong. Issues may also arise if the chemical composition of the surface used in calculations is not appropriate. For instance, the well-cited (2×1) reconstruction on $SrTiO_3$ (100) certainly occurs due to chemisorbed water [15,96,97]. Similarly, an early model for the $c(6 \times 2)$ reconstruction on the same surface assumed that it contained only surface titanium and oxygen, while a more extensive analysis with additional information showed that strontium was also present at the surface [74,80]. In principle one can avoid these pitfalls by performing a global search over different possibilities. However, this currently requires very expensive computation. *Ab initio* methods are also prone to uncertainties due to the limitations of many density functionals when describing strongly correlated oxides [98].

What is badly needed are ways to both predict and judge the reasonableness of specific atomic structures, based upon a chemical approach to complement physics-based ideas such as polarity, which are frequently invoked but unfortunately often fail to

describe experimental results. Efforts to address this line of thinking have been made in the context of the $SrTiO_3$ (100) surface. The idea of polyhedral packing of TiO_5[] units was first proposed with the solution of the $SrTiO_3$ (100) (2 × 1) surface [15]. After these structural units were identified, their specific arrangements were investigated with theoretical DFT calculations, and it was concluded that low-energy arrangements minimized non-bonding oxygen interactions [99]. The bulk concept of bond valence sums was also applied to understanding oxide surfaces [100], addressing local atomic coordination. Additionally, taking these ideas a step farther and calculating hypothetical structures via DFT has led to the identification of multiple structures with similar surface energy. This supports the idea that surfaces can maintain a structure similar to a 2-D network glass with only short-range order if the other previous requirements are fulfilled [11,20,101].

We propose here a more general framework that provides guidelines for understanding oxide surface structures exploiting information from well-established inorganic bulk atomic structures. This approach comes from work by Linus Pauling in 1929 [102], with what have become known as Pauling's rules. These provide simple guidelines that have been shown to work for bulk structures and, as we will show here, can be adapted and applied to oxide surfaces. We acknowledge that this chemical approach to understanding oxide surfaces will be unfamiliar to some readers but appears to be a more appropriate way to approach them.

Being more specific, the body of solved reconstructions on $SrTiO_3$ surfaces is discussed from the perspective of Pauling's rules. The common features of these reconstructions are identified and explained within this framework, revealing similarities in structure across these apparently disparate surfaces. Following this, nanostructures on the $SrTiO_3$ (100) and (110) surfaces are discussed, which represent the first stage of transition from a surface reconstruction to a thin film. Finally, the reconstructions on two other oxide surfaces, $BaTiO_3$ (100) and $LaAlO_3$ (110), are presented.

Before getting further into the details, we need to clarify one important point: what is the meaning of “valence” and “bonding” when it comes to bulk oxides and oxide surfaces, and how is this different from ideas such as polarity and charge; valence lies at the heart of Pauling's rules.

2. Valence, charge, and polarity

In the original work Pauling used the term “charge” for atoms, but in the years since this has evolved to the concept of valence which is not the same. This is important, and remains an area where there is substantial confusion and often errors in the literature. In all oxides except a few superoxides or peroxides (which contain O_2^{2-} ions), the valence state of oxygen is 2-. Note that the sign is written after the number, which is the convention. The actual electrostatic charge on the oxygen is generally smaller than this, for instance −1.5, where the sign is on the other side of the number. Valence is typically considered for oxides in terms of the bond valence sum (BVS) model [100,103–105]. In the limit of a fully ionic model, valence and the electrostatic charge are the same, but of course the full ionic model is unrealistic in almost all cases. Valence is a readily available experimentally measurable number, whereas the actual charge is less available and varies depending upon how the electron density is partitioned to the different atoms. Essentially every spectroscopic technique used in surface science, for instance x-ray photoelectron spectroscopy, Auger spectroscopy, electron energy loss, x-ray adsorption spectroscopy compares the positions of spectroscopic peaks to oxide standards of known *valence*, not known *charge*.

In the BVS approach, the valence depends only the ions involved and the bond distance. Shorter bonds have higher valence relative to the typical bond length between the two species in question. This is calculated according to the equation:

$$BV = \exp((R_0 - R)/b)$$

where R is bond distance, R_0 a standard bond distance for the two ions derived from structural analysis of multiple known materials, and b is an empirically derived constant normally equal to 0.37. If the valence of the cation is known (or assumed), then valence-specific values for R_0 and b can be used; if it is not known then more general values can be used. The relevant values can be found in many databases.

For any given ion the BVS is equal to the sum of all bond valences for the bonds it participates in where cations are treated as positive values and anions as negative:

$$|BVS| = \sum_{all\ bonds} BV$$

A lower BVS indicates a more reduced species while a higher one indicates a more oxidized one. A lower magnitude indicates lower coordination while a higher magnitude value indicates higher coordination. In this way the environments of specific ions can be investigated and compared, and the overall structural stability can be evaluated based on the deviation of the BVSs from expected values for all atoms (typically integers) in a given unit cell. These deviations are often used to check the reported structure of bulk oxides determined by methods such as x-ray diffraction, and work similarly for surfaces [106].

The BVS approach applies to any material. It is most frequently discussed for oxides and other insulating ionic materials, but its concepts are universal and can be applied to any type of crystalline material and also organic compounds. For organic compounds the concepts of valence are so widely accepted that it is sometimes forgotten that this is the same approach that is used for other materials. It applies equally well to metallic oxides as it does to reduced oxides, and can be used for ones with different and, in some cases, multiple valences such as Fe_3O_4, or even fractional valences.

Prior work has demonstrated that Pauling's second rule [100], which yields the BVS model [100,103–105], can qualitatively predict the relative energy of a surface structure consistent with DFT relaxation and experimental evidence. Information obtained from a BVS analysis also indicates whether atoms are over- or under-bonded, giving additional insight into adsorption or disassociation behavior. This offers a quick tool for evaluating a proposed structure and can result in significant savings in terms of computation. However, the BVS model by itself does not offer any predictive capabilities in terms of generating a possible structure to be tested as it ignores the important non-bonded repulsions.

A question that could be asked is how valence connects to the

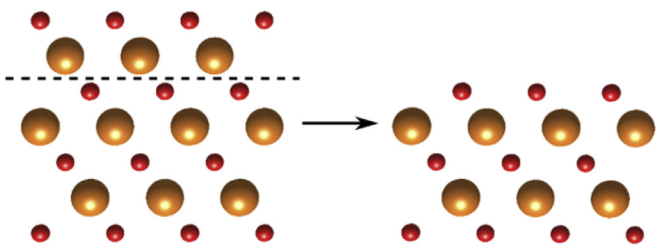

Fig. 1. MgO crystal structure shown such that (111) planes are parallel to the dotted line. Truncation above a bulk oxygen layer leads to the surface visualized on the right. Mg atoms are orange, and oxygen are red. (For interpretation of the references to color in this figure legend, the reader is referred to the Web version of this article.)

ideas of polarity and polarity compensation mechanisms that are often used to analyze and rationalize the structure of polar surfaces. The answer is that it does connect, but there are common misconceptions in the literature. Too often the valence of atoms has been considered as fixed, and interpreted as if it is a charge. For instance, the MgO (111) surface has alternating layers of magnesium and oxygen. Suppose we truncate the surface after, for instance, an oxygen plane as shown in Fig. 1, and do not allow for any relaxations.

If we misinterpret the material as if the valence is fixed at Mg^{2+} and O^{2-} and these are true electrostatic charges, then there is an unbalanced charge and dipole at the surface which nominally has infinite energy. This is incorrect. Since the oxygen atoms have only half the number of magnesium neighbors their valence is not 2-, it is 1-. The surface is anomalously oxidized, but does not have a net charge or dipole. Contracting the magnesium-oxygen distances at the surface will lead to the oxygen having valences of 2-, at the expense of producing chemically unreasonable Mg 3+. If one similarly truncates after a magnesium plane then the magnesium at the surface is Mg^{1+}, which is unreasonably reduced. By definition, the total valence of any system of cations and anions is zero, and there are no unbalanced charges (unless the system is deliberately charged by some other means).

In the context of modern valence theory, the issue for polar surfaces such as MgO (111) is not how its polarity is compensated, but rather how does the structure rearrange from the simple bulk termination which has unreasonable valences corresponding to absurd degrees of oxidation or reduction, to one where the valences conform to the expectations of solid state chemistry. In some cases this may be associated with reduced species (e.g. Fe^{2+} rather than Fe^{3+}). However, to obtain a reduced species the local co-ordination has to change – lower coordination and/or longer bonds.

3. Pauling's rules

We now turn to a general explanation of the rules as they relate to surfaces, before going into specific cases later in this manuscript. Pauling's rules [102] were originally stated as follows:

1. "A coordinated polyhedron of anions is formed about each cation, the cation-anion distance being determined by the radius sum and the coordination number of the cation by the radius ratio."
2. "In a stable coordination structure the electric charge of each anion tends to compensate the strength of the electrostatic valence bonds reaching to it from the cations at the centers of the polyhedral of which it forms a corner; that is, for each anion"

$$\zeta = \Sigma_i \frac{z_i}{v_i} = \Sigma_i s_i$$

where ζ is the charge of the anion, z_i is the electric charge of a cation, v_i its coordination number, and s_i the strength of the electrostatic valence bond.

3. "The presence of shared edges, and particularly shared faces, in a coordinated structure decreases its stability; this effect is large for cations with large valence and small coordination number, and is especially large in case the radius ratio approaches the lower limit of stability of the polyhedron."
4. "In a crystal containing different cations those with large valence and small coordination number tend not to share polyhedron elements with each other."
5. "The number of essentially different kinds of constituents in a crystal tends to be small."

In bulk oxides and other compounds, these rules have held up very well over the years. The only one where there has been a change is the second rule, which Pauling originally stated in terms of "charge". As discussed above, the modern approach is to refer to this in terms of valence, which is not the same as the electrostatic charge (although this point is often confused).

A good starting place is Pauling's concise fifth rule, "The number of essentially different kinds of constituents in a crystal tends to be small." This implies that the number of unique structural units making up a surface structure is also small; it can be broken down and described by a small set of individual "puzzle pieces" so one does not have to consider all possible combinations.

Next comes a description of the structural units themselves, based on Pauling's first rule. These units consist of a cation surrounded by anions (oxygen for oxides), whose arrangements are well-described by regular chemical polyhedra. For example, the bond lengths and angles in a four-fold coordination polyhedron are as similar as possible to those of an ideal tetrahedron, and so on for higher coordinations. The radius ratio portion of the rule indicates what polyhedron is most stable for a given AO_x, i.e. how many oxygens it is coordinated with in its most stable configuration. The atomic radii of the anions and cations in a crystal can be used to calculate this configuration according to the standard equation:

$$\rho = \frac{r^+}{r^-}$$

where different values of ρ correspond to the lowest-energy coordination for the ion. While ionic radii depend on the specific coordination of an atom, even using the reference values provided for crystal ionic radii assumed to be 6-coordinated allows the periodic trends to be examined at a level sufficient for structure prediction. Even using the average ionic radii for a given ion this rule can be useful: for example it accurately predicts that the Cl ion will be 6-coordinated in NaCl $\left(\rho = \frac{r^+}{r^-} = \frac{1.16\ pm}{1.67\ pm} = 0.69\right)$ but 8-coordinated in CsCl $\left(\rho = \frac{r^+}{r^-} = \frac{1.81\ pm}{1.67\ pm} = 1.08\right)$ [107]. This rule extends to the surface, where the same polyhedral units are present.

The next guideline concerns the spatial organization of units with respect to one another and combines Pauling's third and fourth rules. In a surface structure, cation polyhedra sharing faces are higher in energy than those sharing edges, which are higher in energy than those sharing corners. This effect is more pronounced for cations with higher valence and smaller coordination numbers; e.g., a tetrahedral unit of TiO_4, where the Ti species is Ti^{4+}, is less likely to share a face than it is to share an edge with another TiO_4 unit compared to an octahedrally coordinated TiO_6 unit. Furthermore, a cation of lower valence (such as Sr^{2+} in $SrTiO_3$), is more likely than $Ti^{4+}O_x$ polyhedra to share faces or edges due to its lower valence and higher coordination. Pauling did not comment on "naked" polyhedra where nothing is shared; these are less common in the bulk except for crystals with monovalent anions such as OH^- or Cl^-; they should be similarly rare for surfaces except those with monovalent species. By inference, naked polyhedra will be higher in energy.

Of some relevance later, the above rules implicitly lead to Ising or Potts models (see also [11]). To have polyhedral coordination with atoms in the bulk, there are only certain sites that can be occupied, and these will form a lattice. If these sites are only occupied by one type of structural unit, then the surface can be described as an Ising model – the sites are either occupied or not, a binary choice. When there are more structural units the corresponding term is a Potts model. Ideas such as Potts models for

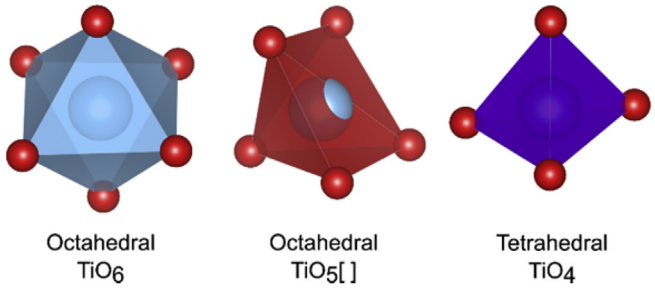

Fig. 2. Idealized coordination environments for TiO_x showing (from left to right) octahedral TiO_6, octahedral $TiO_5[]$, and tetrahedral TiO_4.

simpler surface phenomena such as chemisorption or melting are well known in the literature (e.g. Refs. [108–113]), and arise naturally because of Pauling's rules and the coordination to the underlying bulk.

In the following sections we will show that these guidelines are obeyed for known oxide surface structures, and therefore place restrictions on the lowest energy atomic arrangements of an unknown oxide surface. In cases where there are many different surface structures as a function of composition, they can be used to identify the building blocks of reconstructions and extract more specific rules for their arrangement. They also provide insight into the many phenomena occurring at surfaces during the formation of nanostructures and thin film growth. The following corollary holds: structures that appear to violate the rules are either the rare exception or incorrect.

4. Case analyses

The specific examples that will be discussed are reconstructed (100), (110), and (111) surfaces of $SrTiO_3$, $SrTiO_3$ nanostructures, film growth on $SrTiO_3$ (100), reconstructions on $BaTiO_3$ (100), and reconstructions on $LaAlO_3$ (110). Before discussing these, the universal features of all solved reconstructions on $SrTiO_3$ will be outlined.

All experimentally solved reconstructions on $SrTiO_3$ (to date) are charge and valence neutral, can be represented by the formula $n SrTiO_3 \bullet m TiO_2$, and have Ti-rich outer layers. Even on the polar surfaces of $SrTiO_3$ (110) and (111) this formula is followed, resulting in valence-compensated surface structures.

There are universal features that are related to Pauling's rules:

1. Pauling's fifth rule implies that a structure will minimize the number of different arrangements of its atoms. This leads to structures with higher symmetry being lower in energy. This is because increasing symmetry yields fewer inequivalent atomic positions in a unit cell, and thus fewer bonding environments.
2. All the surfaces can be considered in terms of either an Ising model, if there are two structural units, or Potts models when there are more than two. This connects to Pauling's fifth rule.
3. According to the radius ratio explanation in Pauling's first rule, a 6-fold octahedral coordination with oxygen (TiO_6) is the lowest-energy arrangement for Ti atoms. As the density of Ti atoms on a given surface decreases, Ti adopts coordinations with fewer oxygen atoms to maintain a continuous, periodic network on the surface e.g. 5-fold octahedral ($TiO_5[]$) and 4-fold tetrahedral coordinations (TiO_4). The 5-fold octahedral coordinations are based on TiO_6 units with a single oxygen vacancy. The various coordinations TiO_x can adopt are shown in Fig. 2, and the bond lengths and angles of Ti–O in each polyhedron are optimal when they are as similar as possible to the ideal polyhedron; this reduces the non-bonded repulsions between the oxygen atoms.
4. The lowest-energy sites for a TiO_x unit on the $SrTiO_3$ surface are those that are a continuation of the bulk ordering. These are referred to as “natural Ti sites” herein. These sites obey Pauling's third and fourth rules by minimizing the number of shared faces with cation polyhedra in the lower bulk layers.
5. The oxygen atoms are always coordinated to either two or three cations-three mainly when they are coordinated to strontium. This follows from rules 1–3 and partially 4. For instance, if only corner-sharing occurs, then the oxygen can only be bonded to two cations. Three-fold coordination requires edge-sharing which is more likely with lower valence atoms such as strontium.

4.1. $SrTiO_3$ (100)

The surface of $SrTiO_3$ (100) possesses many identified reconstructions. Those that have been reported and solved are summarized in Table 1 below. Of these, the solved reconstructions, shown in Fig. 3, will be discussed in terms of Pauling's rules.

As evidenced by Fig. 3, all reported structures decorate the bulk-like TiO_2-plane termination of $SrTiO_3$. Of these reconstructions, the (2×1), (2×2)A, (2×2), c(4×2), and $(\sqrt{13} \times \sqrt{13})$R33.7° are formed in what has become known as a Ti double-layer structure, where a single layer of $TiO_5[]$ units are located on top of the bulk-like TiO_2 plane. These $TiO_5[]$ have four oxygen atoms in the same plane or slightly above the central Ti. Two of these oxygens, at opposite ends of the polyhedron, are shared with bulk-like TiO_6 in the layer below. The remaining oxygens are shared with other $TiO_5[]$ in the surface layer. It is possible for these oxygen atoms to be shared with more than two Ti, but this configuration is less favorable, as discussed previously. Each $TiO_5[]$ also shares an oxygen atom that sits below the central Ti with two bulk-like TiO_6 below. The preceding description can be presented as a symbolic representation of the Ising model, as shown in Fig. 4, where the (2×2) reconstruction is used as an example. It would also be possible to

Table 1
Reconstructions on $SrTiO_3$ (100) from the literature.

Reconstruction	Structure Status	Pictured	Reference/s
(1×1)	Observed, models proposed	n/a	[47,57,58,62]
(2×1)	Observed and solved	Fig. 3 (c)	[15,47,57,59,62,71]
(2×2)	Observed and solved	Fig. 3 (b)	[57,58,62,67,72,99]
(2×2)A	Observed and solved	Fig. 3 (a)	[57,58,62,67,72,79]
c(4×2)	Observed and solved	Fig. 3 (f)	[66,70,71]
c(4×4)	Observed, models proposed	n/a	[62,70,72]
(4×4)	Observed, models proposed	n/a	[72]
c(6×2)	Observed and solved	Fig. 3 (d)	[59,66,70,71,74,80]
$(\sqrt{5} \times \sqrt{5})$R26.6°	Observed, models proposed	n/a	[60,68,69,72]
$(\sqrt{13} \times \sqrt{13})$R33.7°	Observed and solved	Fig. 3 (e)	[20,59,72]

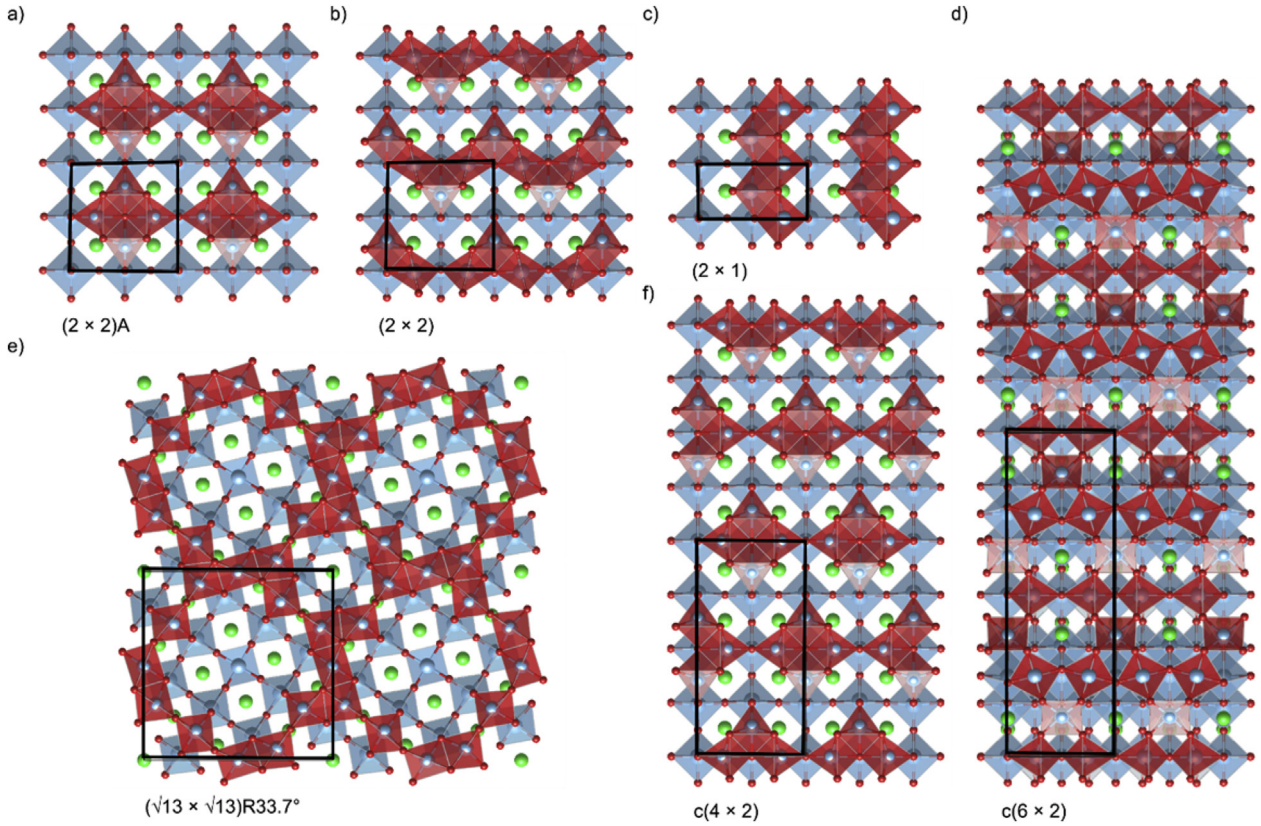

Fig. 3. Atomic structure of solved reconstructions on the $SrTiO_3$ (100) surface showing (a) (2 × 2)A, (b) (2 × 2), (c) (2 × 1), (d) c(6 × 2), (e) ($\sqrt{13} \times \sqrt{13}$)R33.7°, and (f) c(4 × 2). TiO_5[] units are red, TiO_6 light blue. Sr atoms are green, Ti are blue, and oxygen are red. (For interpretation of the references to color in this figure legend, the reader is referred to the Web version of this article.)

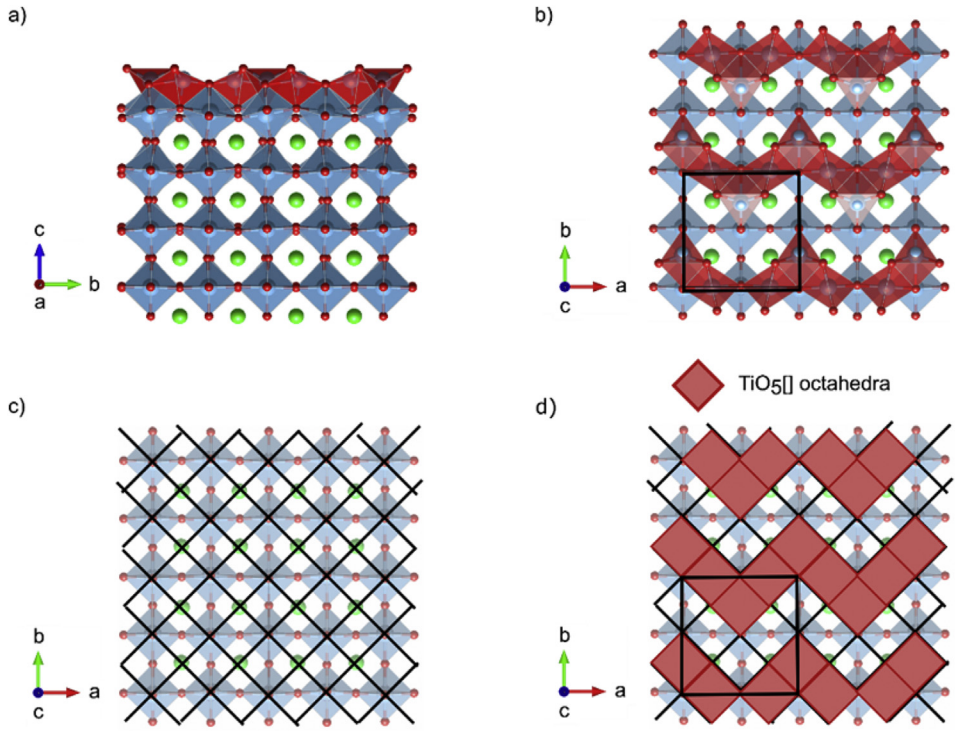

Fig. 4. Atomic structure of the solved (2 × 2) reconstruction on $SrTiO_3$ (100) viewed from the a-axis (a), and c-axis (b). In (c) a square grid is imposed on the underlying bulk TiO_2 layer and in (d) the reconstruction is represented by red squares showing placement of TiO_5[] units on this grid. (For interpretation of the references to color in this figure legend, the reader is referred to the Web version of this article.)

Table 2
Reconstructions on $SrTiO_3$ (110) from the literature.

Reconstruction	Structure Status	Pictured	Reference/s
$(n \times 1)$ $(n = 2, 3, 4, 5, 6, \infty)$	Observed and solved	Fig. 5 (a – e, g, h)	[48,77]
(5×1)A	Observed and solved	Fig. 5 (f)	[78]
$(2 \times n)$a $(n = 2, 3, 4, 5, 6, \infty)$	Observed and solved	(4×2)a in Fig. 11	[81]
$(2 \times n)$b $(n = 2, 3, 4, 5, 6, \infty)$	Observed and solved	n/a	[81]
(2×5)	Observed	n/a	[63]
(3×4)	Observed	n/a	[63]
c(2×6)	Observed, models proposed	n/a	[61]
(4×4)	Observed	n/a	[63]
(6×4)	Observed	n/a	[63]
(4×7)	Observed	n/a	[63]

represent these examples by further distinguishing between inequivalent TiO_5[] octahedra, resulting in a Potts model with more units present, but in this case the different orientations are similar enough in terms of their atomic positions to allow the simplifying generalization made below.

In Fig. 4 (a) and (b) the reconstructed surface is viewed along two different axes, with the surface perpendicular to the c-axis. A grid can be drawn, as shown in Fig. 4 (c), on the bulk-like TiO_2 layer. Fig. 4 (d) shows how the reconstruction is codified into a symbolic representation with one type of structural unit, TiO_5[]. These units occupy positions such that the Ti atom sits above the oxygen shown in the center of the imposed grid. Four additional oxygen atoms defining the TiO_5[] unit are located laterally near the positions of grid intersections, some closer to vacuum than the Ti atom. These are represented by the red squares in Fig. 4 (d). The surfaces can be considered using a binary Ising model since there are only two options for occupation of each grid position-either a TiO_5[] unit above the bulk layer or nothing.

Pauling's fifth rule suggests that the number of different structural units is small. This is evidenced by the TiO_5[] units, the only coordination environment needed to describe these reconstructed surfaces. Pauling's first rule indicates that the relaxed positions of atoms in the TiO_5[] units will bring them as close to ideal octahedra as possible.

TiO_5[] units occupy the grid shown in Fig. 4 (c). To satisfy the third and fourth rules Pauling outlined, they do not share faces with other TiO_x units. The sharing of edges between TiO_5[] is also minimized. An increase in Ti-excess coverage in these reconstructions leads to a more densely packed network of TiO_5[] units (and more edge sharing), but this minimization rule is still followed.

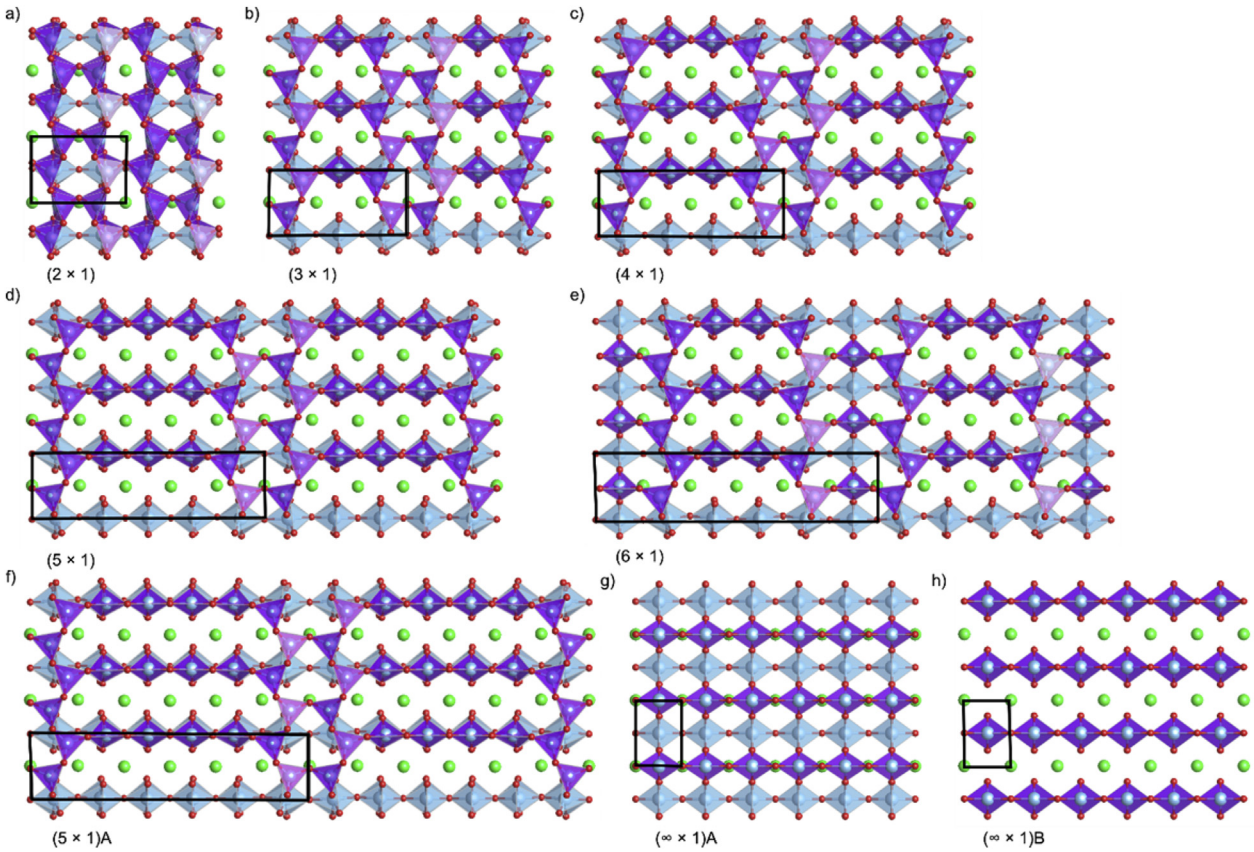

Fig. 5. Atomic structure of solved reconstructions on the $SrTiO_3$ (110) surface showing (a) (2×1), (b) (3×1), (c) (4×1), (d) (5×1), (e) (6×1), (f) (5×1)A, (g) $(\infty \times 1)$A, and (h) $(\infty \times 1)$B. TiO_6 are light blue, TiO_4 are purple. Sr atoms are green, Ti are blue, and oxygen are red. (For interpretation of the references to color in this figure legend, the reader is referred to the Web version of this article.)

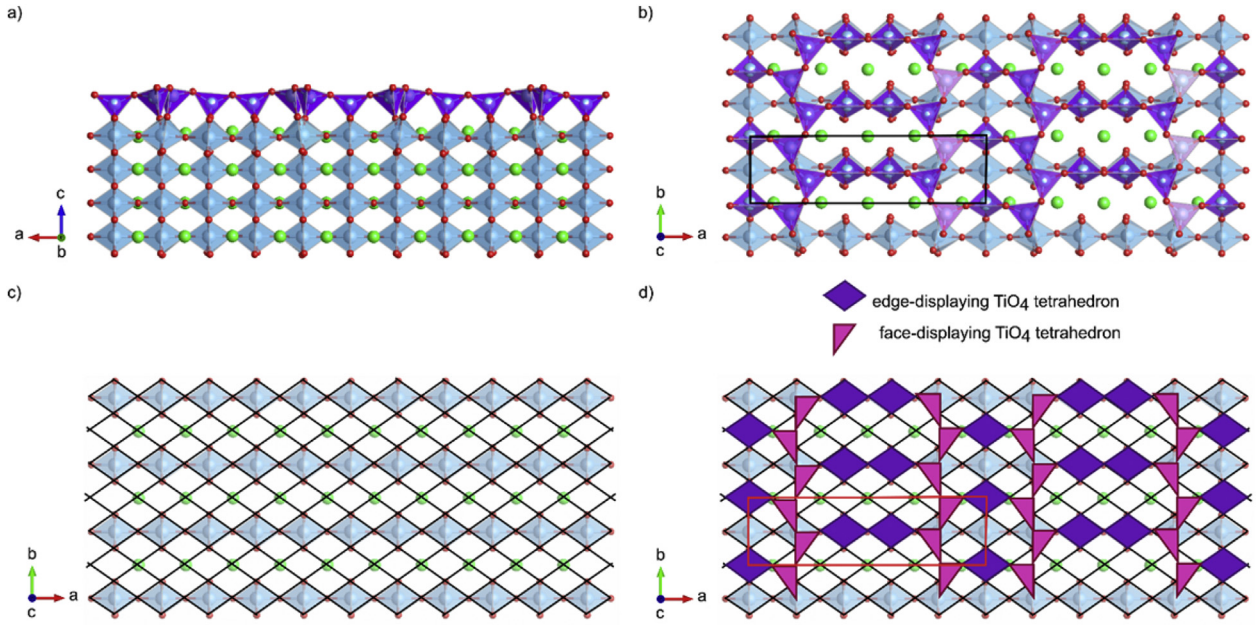

Fig. 6. Atomic structure of the solved (5×1)A reconstruction viewed from the b-axis (a), and c-axis (b). In (c) a diamond grid is imposed over the bulk layers below and in (d) the reconstruction is represented by purple diamonds and pink triangles showing placement of two different orientations of TiO_4 units. (For interpretation of the references to color in this figure legend, the reader is referred to the Web version of this article.)

4.2. $SrTiO_3$ (110)

While the idealized (100) termination is charge and valence neutral, the polar $SrTiO_3$ (110) surface possesses a macroscopic electrostatic dipole from the alternate stacking of $(SrTiO)^{4+}$ and $(O_2)^{4-}$ layers. To be feasible, a surface reconstruction must stabilize (eliminate) this dipole and also lead to a valence neutral structure; remember that valence and charge are different. The array of structures observed on $SrTiO_3$ (110) include those summarized in Table 2. Those with solutions include the homologous $(n \times 1)$ series (where $n = 2, 3, 4, 5, 6, \infty$) [77], a related (5×1) reconstruction [78], and the two families of larger $(2 \times n)$ (where $n = 2, 3, 4, 5, 6, \infty$) nanostructures, which will be discussed later. The $(n \times 1)$ series and related (5×1) structure are shown in Fig. 5 below [81].

Each structure in Fig. 5 is built on the same template: if $SrTiO_3$ (110) is thought of as alternating layers of $(SrTiO)^{4+}$ and $(O_2)^{4-}$, the bulk $SrTiO_3$ (110) base terminates on a $(SrTiO)^{4+}$ layer. Above this layer, tetrahedral TiO_4 units make up the reconstruction. Each TiO_4 unit shares either one or two oxygens with the Ti atoms below such that there is a bulk-like $(O_2)^{4-}$ layer between the reconstructed Ti-atoms and those immediately below; it is a Potts model structure, as there are two different tetrahedral structures plus nothing-a total of three structural units. The remaining oxygen atoms in the TiO_4 units are in the same plane or closer to vacuum than the central Ti atom. This description is turned into the symbolic representation of the Potts model shown in Fig. 6. The (5×1)A reconstruction is used as an example demonstrating unit types and placement sites.

In Fig. 6 (c) the surface of $SrTiO_3$ (110) is shown with a diamond grid imposed over the bulk-like $(SrTiO)^{4+}$ layer. Fig. 6 (d) shows the (5×1)A reconstruction codified into its symbolic representation. Each TiO_4 has bond lengths and angles as close to the ideal tetrahedra as possible. Edge-displaying TiO_4 (ED-TiO_4) are indicated by purple diamonds. ED-TiO_4 occupy sites such that their Ti atom is in a grid space's center. The positions of oxygen in ED-TiO_4 occur at roughly the corners of the imposed grid diamonds. Two of the oxygens, those at the closest opposite diamond corners, are shared with TiO_6 below. The remaining two are shared with other TiO_4 in the same layer. Face-displaying TiO_4 (FD-TiO_4) are represented by pink triangles. The corners of these triangles represent the positions of oxygen atoms in the outermost layer. FD-TiO_4 occupy the grid such that one of their corners is at a grid intersection (one of the two intersections at the furthest opposite diamond corners) and the other two corners are at the center of grid diamonds. The Ti atom of each FD-TiO_4 is in the center of the triangle. They have one oxygen atom shared with TiO_6 in the layer below, beneath the central Ti atom. Its position is indicated by grid intersections (one of the two intersections at closer opposite diamond corners).

To satisfy Pauling's fifth rule the number of structural units must be as small as possible. This is the case we see; only ED-TiO_4 and FD-TiO_4 units make up these reconstructions. The observed placement of ED-TiO_4 and FD-TiO_4 dictated by the grid ensures that TiO_4 (in particular ED-TiO_4) occupy positions similar to the bulk-like TiO_6 below. This is favorable from an energy standpoint-if Pauling's fifth rule is taken to its extreme then one expects that surface positions/coordinations mimicking those of the bulk are lower in energy. As opposed to the $SrTiO_3$ (100) surface, where TiO_5[] are the basic units, these reconstructions have a lower TiO_x surface density. Due to this, TiO_4 tetrahedra are the lowest energy configuration which also creates a self-supporting network. This implies that increasing

Table 3
Reconstructions on $SrTiO_3$ (111) from the literature.

Reconstruction	Structure Status	Pictured	Reference/s
(1×1)	Observed	n/a	[64,65,73]
$(9/5 \times 9/5)$	Observed	n/a	[9,10]
(2×2)a	Observed and solved	Fig. 7 (d)	[11]
(2×2)b	Observed and solved	Fig. 7 (b)	[11]
$(\sqrt{7} \times \sqrt{7})$R19.1°	Observed and solved	n/a	[75,82]
(3×3)	Observed and solved	Fig. 7 (c)	[9–11]
$(\sqrt{13} \times \sqrt{13})$R13.9°	Observed and solved	n/a	[75,82]
(4×4)	Observed and solved	Fig. 7 (e)	[9–11]
(5×5)	Observed	n/a	[10]
(6×6)	Observed	n/a	[9,10]
(1×2) – "Low"	Theoretical low-energy	Fig. 7 (a)	[11,76]
(1×1) – "High"	Theoretical low-energy	Fig. 7 (f)	[11,76]

the TiO_x density would eventually lead to observation of TiO_5[] or TiO_6 units - this is seen in the case of TiO_x nanostructures on the (110) surface, $(2 \times n)$a/b (where $n = 2, 3, 4, 5, 6, \infty$), which will be discussed in a later section.

As the Ti coordination decreases, the adherence to the third and fourth rules becomes more extreme. This is observed in multiple aspects of these surfaces. For instance, sharing faces between TiO_4 would be the most unfavorable arrangement possible, and it is never observed. Also, while ED-TiO_4 share a single edge with the TiO_6 below, they never share edges with other TiO_4 units. This demonstrates the nuance captured by Pauling's rules. ED-TiO_4 can share an edge with a TiO_6 unit because the TiO_6 unit is not as low in coordination, and thus this type of sharing is observed more often than edge-sharing between two TiO_4 units. The tendency to

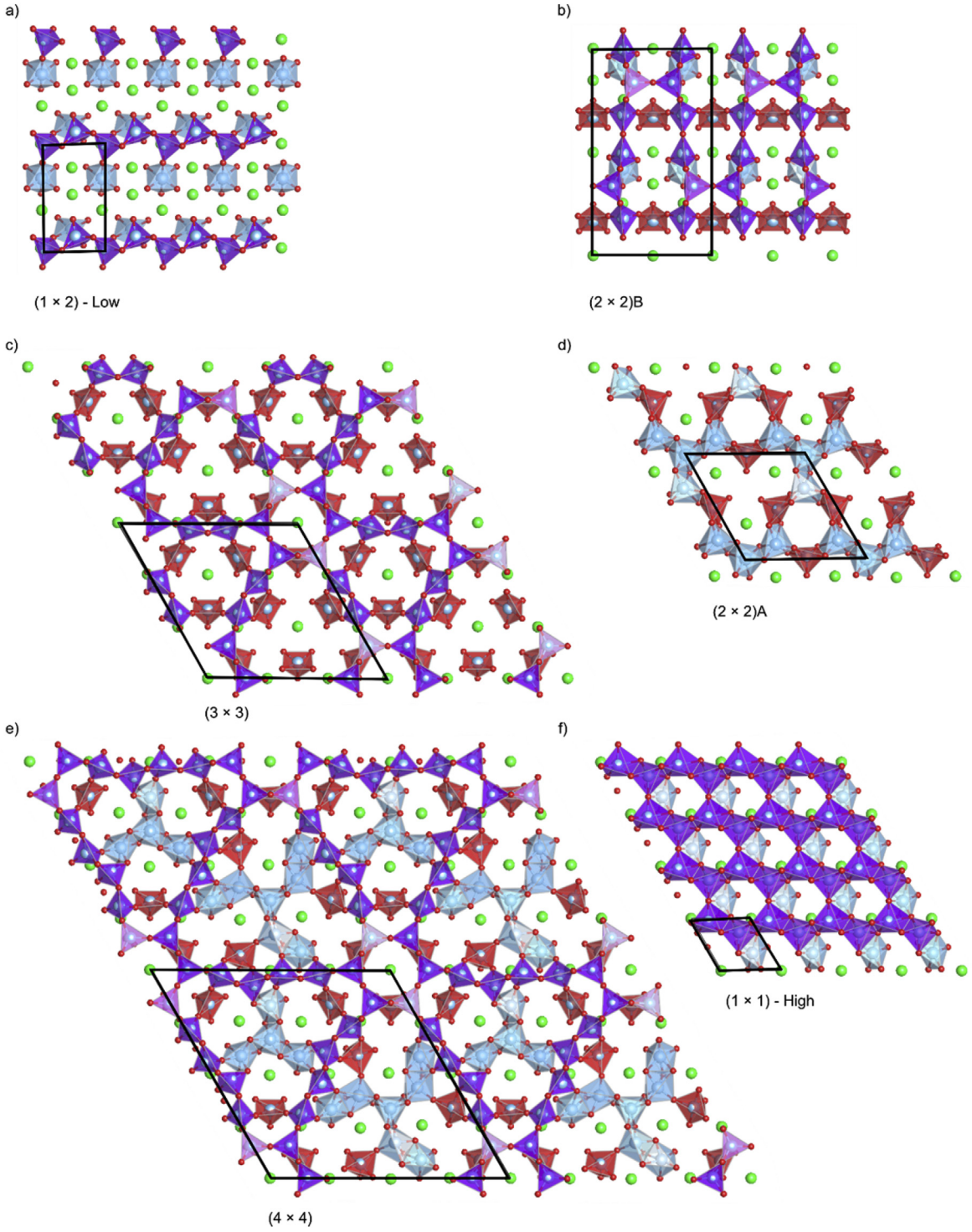

Fig. 7. Atomic structure of solved reconstructions on $SrTiO_3$ (111) surface showing (a) (1×2) – "Low", (b) (2×2)b, (c) (3×3), (d) (2×2)a, (e) (4×4), and (f) (1×1) – "High". TiO_6 units are light blue, TiO_5[] are red, and TiO_4 are purple. Sr atoms are green, Ti are blue, and oxygen are red. (For interpretation of the references to color in this figure legend, the reader is referred to the Web version of this article.)

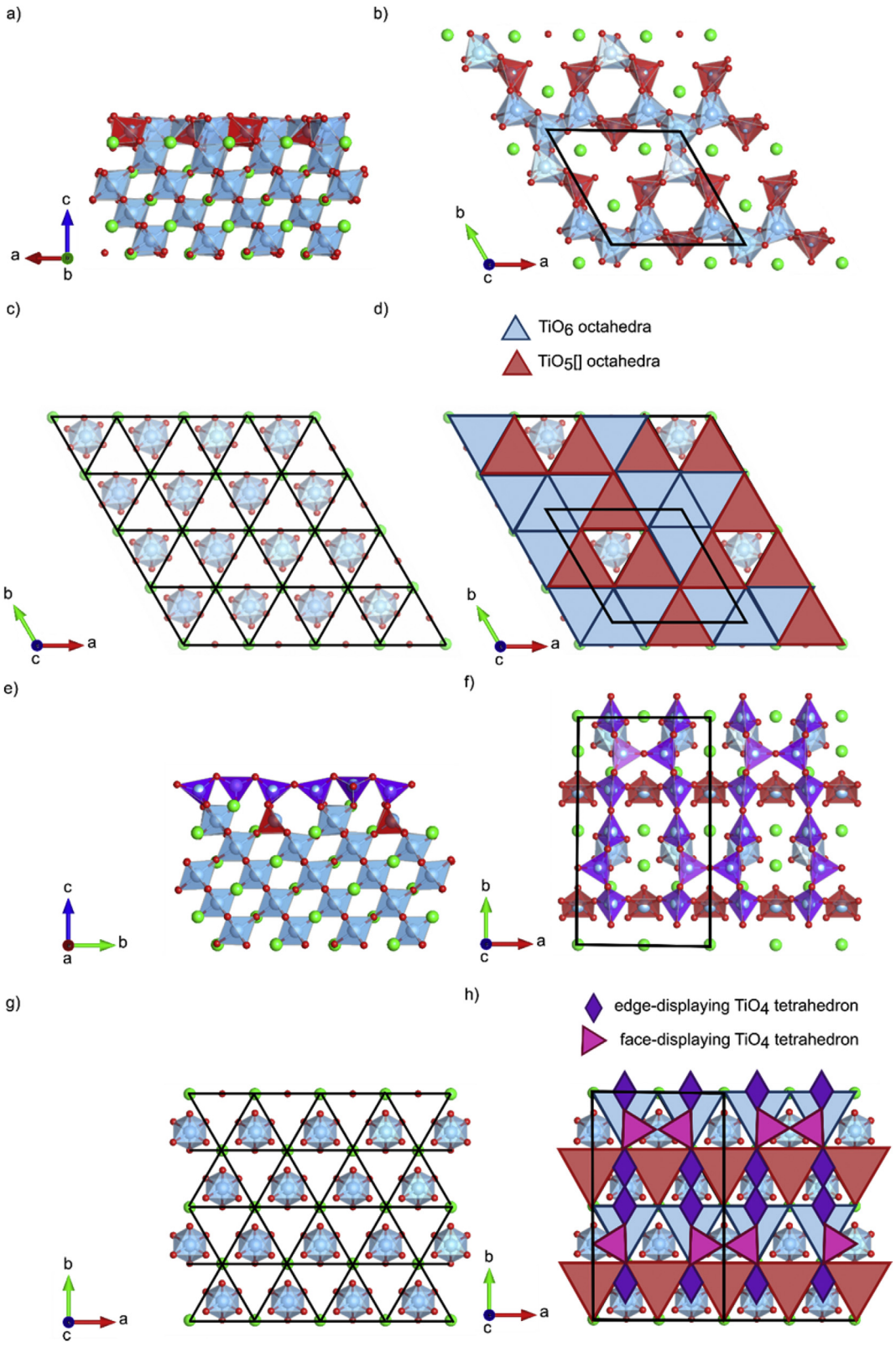

Fig. 8. Atomic structure of the solved (2×2)a reconstruction viewed from the b-axis (a), and c-axis (b). In (c) a triangle grid is imposed over the bulk layer below and in (d) the reconstruction is represented by blue and red triangles showing placement of TiO_6 and TiO_5[] units, respectively. Atomic structure of the solved (2×2)b reconstruction viewed from the a-axis (e), and c-axis (f). In (g) a triangle grid is imposed over the bulk layer below and in (h) the reconstruction is represented by blue and red triangles showing placement of TiO_6 and TiO_5[] units, respectively and purple triangles and diamonds showing placement of TiO_4 units. (For interpretation of the references to color in this figure legend, the reader is referred to the Web version of this article.)

minimize the number of shared edges on this surface also explains why these reconstructions appear to be "bridging" above the bulk material whereas TiO_5[] on the (100) face are nestled closely with the layers below. The TiO_5[] of the (100) surface are more likely to share edges since their coordination is higher. Finally, sharing corners between TiO_4 units is frequently observed. This type of sharing is expected since it is the lowest in energy.

There are some positions where TiO_4 units do not occur. These positions are avoided because they would not minimize face and edge sharing, or because of their proximity to Sr atoms. Having a Ti atom too close to a Sr atom would lead to unfavorable cation-cation repulsion.

4.3. $SrTiO_3$ (111)

The $SrTiO_3$ (111) surface is the most complex and least-studied of the three common terminations. This surface is polar, similar to (110), and the material can be thought of as a stacking of alternating layers of $(SrO_3)^{4-}$ and $(Ti)^{4+}$. The two-dimensional Bravais lattice of this termination is hexagonal, leading to more complex symmetry in its reconstructions. The structures reported and solved on the $SrTiO_3$ (111) are summarized in Table 3. Of these, the solved reconstructions and selected theoretical low-energy structures with high and low excess-TiO_2 coverage are shown in Fig. 7 [11,76].

In Fig. 7 the common base for all the reconstructions is a bulk-like $(SrO_3)^{4-}$ layer. On top of this, reconstructions are made up of one or two Ti-containing layers. There are more structural units, so this is a Potts model system. A single Ti-layer reconstruction is shown in Fig. 7 (d). It is composed of TiO_6 and TiO_5[] units on top of the bulk-like $(SrO_3)^{4-}$ plane. These units have either two or three oxygens in a plane above the central Ti, closest to vacuum. They share three oxygens with the TiO_6 units below, ensuring the same stoichiometry of the $(SrO_3)^{4-}$ layer as in the bulk. All of the other reconstructions shown are double-layered in nature. In the layer directly above the $(SrO_3)^{4-}$ they have the same construction as the single-layered reconstruction. The Ti atoms closest to vacuum are present in TiO_4 units, similar in coordination to those on the $SrTiO_3$ (110) surface, having the same ED-TiO_4 or FD-TiO_4 nature. These reconstructions can be represented by the symbolic Potts model shown in Fig. 8. Fig. 8 illustrates two examples, the (2×2)a in Fig. 8 (a–d) and the (2×2)b in Fig. 8 (e–h) to highlight differences between a single Ti-layer reconstruction and a double Ti-layer reconstruction. The Potts model for the single Ti-layer reconstruction is made up of three units: TiO_6, TiO_5[], and an "empty" unit. For the double Ti-layer reconstruction, the Potts model has five units: TiO_6, TiO_5[], ED-TiO_4, FD-TiO_4, and an "empty" unit.

As Fig. 8 (c) and (g) show, a triangular grid can be imposed over the bulk-like $(SrO_3)^{4-}$ layer. A single TiO_x-layer reconstruction is shown in Fig. 8 (a–d). TiO_6 (blue triangles) or TiO_5[] (red triangles) occupy any space on this grid-their Ti atom sits roughly in its center. The oxygens shared with the $(SrO_3)^{4-}$ layer occur at bulk-like positions. The two or three oxygens closest to vacuum (in TiO_5[] or TiO_6) are shared among two TiO_x units and occur at roughly the center points of the triangle's sides, offset in the a and b directions from the oxygens below to adopt a more-ideal polygon. A double TiO_x-layered reconstruction is shown in Fig. 8 (e–h). Placement of TiO_6 and TiO_5[] units in these reconstructions is the same as those of the single-layer reconstruction. However, the outermost oxygen atoms in TiO_6 or TiO_5[] units can be shared by TiO_x in the same layer or with TiO_4 in the layer above. The possible positions of ED-TiO_4 (purple diamonds) and FD-TiO_4 (pink triangles), similar in shape and oxygen-sharing to those on the (110) surface, are all illustrated in the example shown. In all TiO_4 units, the central Ti atom occurs at the center of the diamond or triangle representation. ED-TiO_4 tetrahedra occur on two sites. On one site, the furthest opposite corners of its diamond (oxygen atoms closest to vacuum) are over a grid intersection (above a bulk-like Sr site) and in the center of a grid triangle (above a bulk Ti site). The other site has the two furthest opposite corners, both in the center of a grid triangle, such that one is over a bulk Ti site and the other over a Ti-site occupied by the first TiO_6/TiO_5[] layer. FD-TiO_4 units occur such that one corner of the displayed face is on a grid intersection, above a bulk-like Sr site, while the other two corners of the displayed face are at the center of two different grid triangles. The fourth oxygen is directly below the central Ti.

The variety of structures on $SrTiO_3$ (111) is greater than that of (100) or (110). However, even these reconstructions can be broken down into a small number of coordinated units according to Pauling's fifth rule. These units are also very similar to those on the (100) and (110) surfaces, indicating that Pauling's fifth rule applies in general to a given oxide material. Additionally, TiO_5[] or TiO_6 are arranged such that they are preferentially placed in the natural Ti sites, indicated by open grid triangles without a bulk TiO_6 in Fig. 8 (c) and (g). As explained for the (110) surface, continuing the bulk-like structure minimizes energy on the surface. Pauling's first rule also applies to these surfaces. Here we see a combination of all the possible TiO_x units: in layers where TiO_x density is highest, the most-favorable TiO_6 and TiO_5[] coordinations are adopted with a geometry as close as possible to ideal octahedra. In two-layer TiO_x reconstructions, the outermost layer does not have high enough TiO_x density to support these structures. Instead, the TiO_4 coordination is adopted to create a continuous self-supported network, similar to the (110) surface.

Pauling's third and fourth rules apply here in much the same way as for the (100) and (110) surfaces. The only units to ever share polyhedra faces are TiO_6 and TiO_5[], which occasionally share a face with the bulk-like layers below. However, placing these into natural Ti sites reduces the occurrence of this higher-energy configuration. Also, while TiO_6 and TiO_5[] units often share edges, TiO_4 units almost never do, as expected with their low coordination and high valence. The positions at which each of these types of units occur minimize unfavorable sharing of polygon elements.

A unique feature of the (111) surface, shown in Fig. 7 (a), (b), and (d), is removed or added Sr atoms, necessary to satisfying the $n SrTiO_3 \bullet m TiO_2$ condition. In a single Ti-layer reconstruction, Sr atoms are simply removed from the bulk-like $(SrO_3)^{4-}$ layer. For double Ti-layer reconstructions, there are no reported examples where Sr atoms are removed. However, Sr atoms can be added to the outermost TiO_4-containing layer (e.g., (2×2)b in Fig. 7). When Sr are added, it is to octahedral sites either at the corners or centers of grid triangles. This placement ensures a coordination environment as close as possible to that of the bulk, in accordance with Pauling's rules.

4.4. From reconstructed surface to thin film

The TiO_2-rich surfaces of $SrTiO_3$ discussed above provide a robust example for how Pauling's rules apply to perovskite oxides. As we will show, with increasing coverage the same rules apply, and provide the connection to thin film growth.

All reported TiO_2 nanostructures on $SrTiO_3$ have similar structural features and adopt periodic arrangements similar to the $SrTiO_3$ surfaces they are grown on, showing that Pauling's rules apply to heteroepitaxial film growth. The three structures that will be considered in detail are shown in Table 4.

The $c(6 \times 2)$ reconstruction builds off of the TiO_2 plane termination of $SrTiO_3$ (100). It is "thicker" than others on this surface, exhibiting two additional TiO_x layers. It has the usual TiO_5[] units on its top surface with the addition of Sr adatoms. The TiO_5[] units

Table 4
Nanostructures on $SrTiO_3$ from the literature.

Structure	Surface	Pictured	Reference/s
c(6 × 2)	(100)	Fig. 9	[59,66,70,71,74,80]
Diline/Triline	(100)	Fig. 10	[114,115]
(2 × *n*)a/b (n = 2–6 … ∞)	(110)	Fig. 11	[81]

are the same as those in other $SrTiO_3$ (100) reconstructions. The two additional TiO_x layers between the TiO_5[] surface and bulk-like TiO_6 below are fully 6-coordinated TiO_6 octahedra. This structure is shown in Fig. 9, where the placement of atoms in each subsequent layer is highlighted, using both the symbolic Potts model representations introduced earlier for Fig. 9 (e–h) as well as the resulting structure shown in Fig. 9 (a–d). In this Potts model, the three elements are TiO_6, TiO_5[], and an "empty" unit.

Building up the c(6 × 2) is very similar to any reconstruction previously discussed. The same grid, shown in Fig. 9 (e), is drawn and populated with TiO_x units. These have more layers of TiO_x above and adopt a fully coordinated TiO_6 geometry, shown with blue squares in Fig. 9. Taking this layer as the new "base", another grid can be drawn following the same rules as before. The second additional layer of TiO_6 and TiO_5[] units, green squares in Fig. 9, again occupy the same relative atomic positions that TiO_5[] units in a $SrTiO_3$ (100) reconstruction would be expected to. If this layer had another complete layer of TiO_x units above (i.e. every available site filled) all these units would be TiO_6. However, that is not the case, leading to the presence of some TiO_5[]. This layer is then the basis of the final one, where TiO_5[] units (red squares in Fig. 9) are placed on top, again with the same rules as a normal $SrTiO_3$ (100) surface reconstruction. Please note that all of the TiO_x units have similar geometry (either octahedral or TiO_5[]) and their different colors are to aid the reader in determining how far from the surface they are.

This reconstruction contains only TiO_6 and TiO_5[] units, conforming to Pauling's fifth rule. Pauling's first rule determines which of these two coordinations a given Ti atom is in. If there are additional TiO_x units above it, the Ti atom adopts its most stable coordination, TiO_6. If it is a Ti with no TiO_x units above it, the TiO_5[] coordination is adopted-this is illustrated in the layer represented by green squares in Fig. 9 (c) and (g). Furthermore, to accommodate idealized TiO_5[] coordinations while accounting for differences in surface height, some of the units in the layer represented by red squares in Fig. 9 (d) and (h) are shifted slightly in terms of their ideal grid-determined positions. This structure also has a few additional Sr atoms at its surface. Sr adatoms on the surface follow the same placement rules as those on $SrTiO_3$ (111); they are only present in sites allowing an octahedral coordination, agreeing with Pauling's first and fifth rules.

As with the other $SrTiO_3$ (100) reconstructions, this structure minimizes the number of shared edges between TiO_x units. Sharing of corners is favored while sharing of faces is totally avoided, in agreement with Pauling's third and fourth rules.

TiO_2 nanowires, such as the diline and triline reported on $SrTiO_3$ (100), are other structures approaching the thin film regime [114,115]. The TiO_x di/trilines resemble the simpler c(4 × 2) $SrTiO_3$ (100) reconstruction with the typical TiO_5[] units [50]. Between this

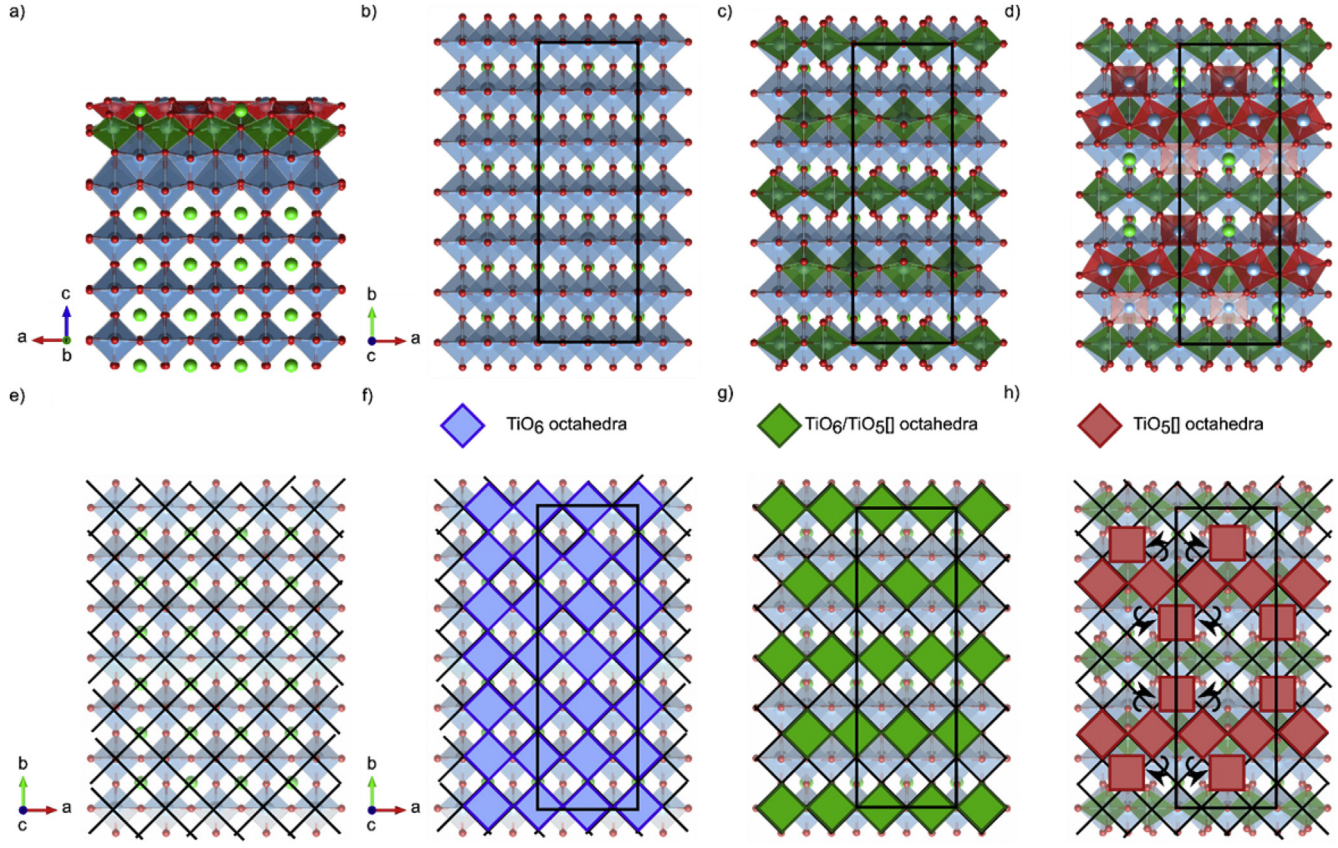

Fig. 9. Atomic structure of the solved c(6 × 2) nanostructure on $SrTiO_3$ (100) viewed from the b-axis (a), and c-axis with a square grid imposed over the bulk layers below (e). In (f) TiO_6 units are placed on top of the bulk, represented by blue squares-the structure of this layer is shown in (b). In (g) TiO_6/TiO_5[] units are represented by green squares and are placed atop those in (b) and (f) – the structure of this layer is shown in (c). In (h) TiO_5[] units are represented by red squares and are placed stop those in (c) and (g) – the structure and tilts of this layer is shown in (d). (For interpretation of the references to color in this figure legend, the reader is referred to the Web version of this article.)

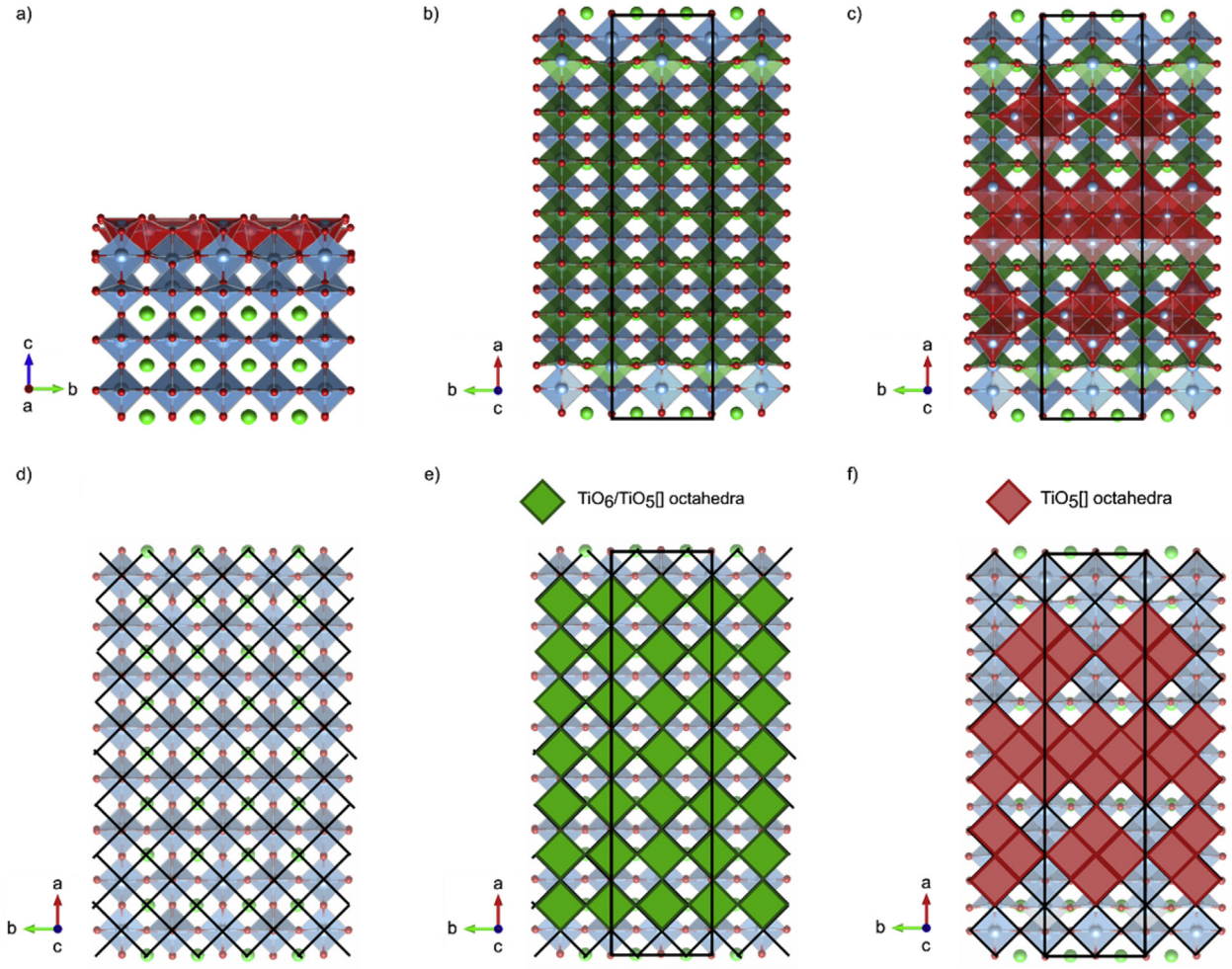

Fig. 10. Atomic structure of the solved triline nanostructure on $SrTiO_3$ (100) viewed from the a-axis (a), and c-axis with a square grid imposed over the underlying bulk (d). In (e) TiO_6 units are represented by blue squares placed atop the grid in (d); the structure of this layer is shown in (b). In (f) TiO_5[] units are represented by red squares placed atop the structure in (b) and (e); the structure of this layer is shown in (c). (For interpretation of the references to color in this figure legend, the reader is referred to the Web version of this article.)

and the bulk-like TiO_6 is a single additional TiO_x layer made up of fully-coordinated TiO_6. This structure is illustrated in the case of the triline structure in Fig. 10. The Potts model shown in Fig. 10 has three elements: TiO_6, TiO_5[], and the "empty" unit.

Building the trilines (and dilines) relies on the same principles as the c(6 × 2) and other reconstructions on the (100) surface. The grid is shown in Fig. 10 (d), and TiO_6 units (blue squares) are placed on it in Fig. 10 (e), following the same pattern of occupation as for the c(6 × 2). The final layer of TiO_5[] units (red squares) are then placed as shown in Fig. 10 (f) and occupy the same relative positions as any other previously-discussed TiO_5[]. Please note that all of the TiO_x units have similar geometry (either octahedral or TiO_5[]) and their different colors are to aid the reader in determining how far from the surface they are, similar to Fig. 9.

Pauling's rules are obeyed by the triline in much the same way as for the normal $SrTiO_3$ (100) reconstructions and the just-discussed c(6 × 2). As this structure simply serves to reinforce these rules, further explanation is not necessary.

TiO_2 nanostructures are not unique to the $SrTiO_3$ (100) surface. Two families, (2 × *n*)a and b (where $n = 2, 3, 4, 5, 6, \infty$), observed on $SrTiO_3$ (110) display the same ordered transition from reconstructed surface to reconstructed thin film [116]. These nanostructures have an additional TiO_x layer when compared to other reconstructions on the (110) surface. On their top surface they display TiO_6 units, rather than the TiO_4 often seen in other (110) reconstructions. Between this surface layer and the bulk below, there is a layer made up of TiO_6 octahedra. These are the same in geometry as those on other $SrTiO_3$ surfaces, and their placement is similar to TiO_4 in other (110) reconstructions. One of these structures, the (2 × 4)a, is shown in Fig. 11, where each layer of the nanostructure is illustrated by the symbolic Ising model in Fig. 11 (d–f) and with the actual structure in Fig. 11 (a–c). Since this structure only has two units, a TiO_6, and an "empty" unit, it can be represented with the binary Ising model.

Building up the (2 × 4)a is the same as other reconstructions on the $SrTiO_3$ (110). The starting base is a bulk-like $(SrTiO)^{4+}$ layer. The grid drawn in Fig. 11 (d) is identical to the ones used before on this surface. It is populated with exclusively TiO_6 units in the same sites that held ED-TiO_4 in other (110) reconstructions. The difference between the ED-TiO_4 seen earlier and these TiO_6 is that these units have oxygens below and above the central Ti atom. These are located at the closest opposite diamond corners (top and bottom corners), so they can be thought of as edge-displaying TiO_6. These are visualized as purple diamonds in Fig. 11 (e). If this layer is then used as the new base, a new grid can be drawn and more TiO_6 placed to form the final layer of the reconstruction, adhering to the same rules. This final layer is visualized as orange diamonds in Fig. 11 (f). This structure also has Sr adatoms, which are placed at

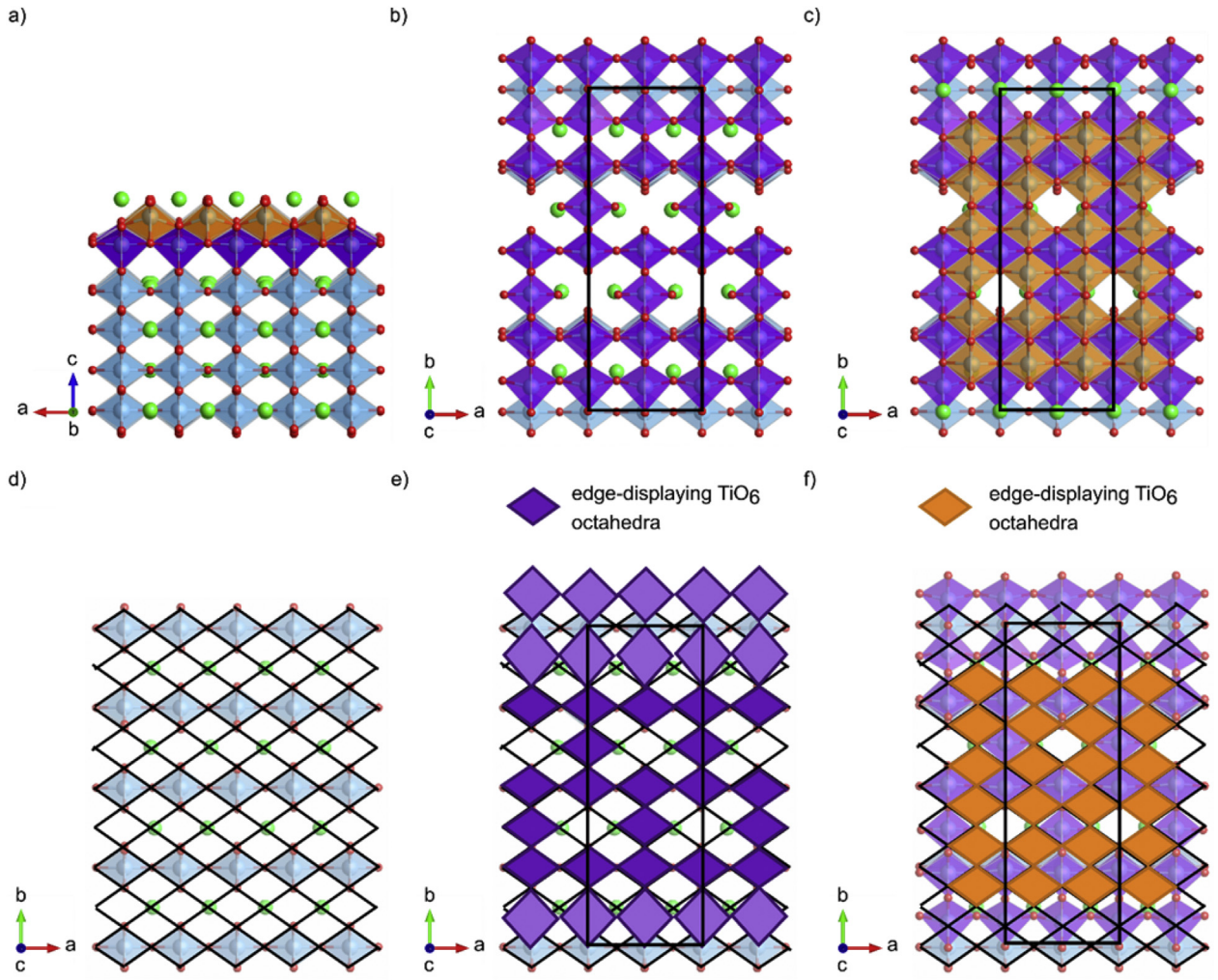

Fig. 11. Atomic structure of the solved (2×4)a nanostructure on $SrTiO_3$ (110) viewed from the b-axis (a), and c-axis with a diamond grid imposed (d). In (e) TiO_6 units are represented by purple diamonds placed atop the grid in (d); the structure and distortions in this layer is shown in (b). In (f) TiO_6 units are represented by orange diamonds placed atop the structure in (b) and (e); the structure of this layer is shown in (c). (For interpretation of the references to color in this figure legend, the reader is referred to the Web version of this article.)

sites with the same in-plane positions as bulk Sr but at the surface.

Pauling's fifth rule is exemplified in these surfaces-the only unit making up these reconstructions is TiO_6. Additionally, its edge-displaying geometry is the same as the bulk-like layers below, making this a particularly low-energy environment. Pauling's first rule gives insight into why the TiO_6 structure is adopted (rather than TiO_4) and some of the shifting seen in the TiO_6 layer is depicted in Fig. 11 (b) and (d). This nanostructure has high TiO_x density. Additionally, many TiO_6 units have another TiO_x unit above them. In this case, it is possible to adopt the most stable coordination according to Pauling's first rule, i.e. octahedral TiO_6. The deviations from the ideal placement shown by the light purple diamonds in Fig. 11 (e) serve to permit this low-energy configuration (as opposed to the higher-energy TiO_4 alternative) and preserve the coordinations as close to the ideal geometry as possible when a fully-occupied TiO_x layer does not exist.

Pauling's third and fourth rules are also obeyed in the placement of TiO_6 on this surface. No faces are shared in any TiO_6 units. Edge sharing is also minimized by the arrangement of these units.

As with the other thin film structures discussed, Sr adatoms decorate the surface at octahedral coordinated positions, in accordance with Pauling's fifth and first rules. In this case, Sr atoms occur above the deviated TiO_6, acting as an additional mechanism for stress relief – they are octahedrally coordinated with a larger bond length than in TiO_6.

4.5. $BaTiO_3$ (100)

Few other perovskite oxide surfaces have been investigated with the same attention as $SrTiO_3$. However, there are surfaces whose reconstructions have been reported that deserve mention. One example of this is $BaTiO_3$ (100).

The structure of $BaTiO_3$ is a perovskite similar to $SrTiO_3$, although $BaTiO_3$ deviates more dramatically from the cubic structure, experiencing a great number of structural transitions with temperature. Since it has the same stoichiometry, B-site cation, and general structure, one would expect its surface reconstructions to have similar structural features to $SrTiO_3$. Of the reported structures for the (2×1) [85], (3×1) [83], $c(2 \times 2)$ [87], $(\sqrt{5} \times \sqrt{5})R26.6°$ [84], $(\sqrt{13} \times \sqrt{13})R33.6°$ [86], and $c(4 \times 4)$ [87], all the proposed solutions have surfaces that are B-site rich, with a similar double-layer structure to the $SrTiO_3$ (100) reconstructions. The similarities between the two end there, however, as these surfaces were all prepared under reducing conditions and have not all been analyzed

by multiple techniques. Since they are reduced, the condition of nBaTiO$_3$•mTiO$_2$ does not hold, allowing for structures with reduced oxygen content, or nBaTiO$_3$•mTiO$_x$ to occur. Proposed models for two of these structures, the c(2 × 2) and c(4 × 4), are shown in Fig. 12.

From Fig. 12 one can see that Pauling's rules are still obeyed to some extent. There are, according to the fifth rule, a small number of structural units in these reconstructions, in this case TiO_6, TiO_5[], and TiO_3. Bulk-like positioning of the first TiO_6/TiO_5[] layer also agrees with the implication from Pauling's rules that surface structures that continue bulk ordering are favorable. The coordination of the TiO_6 and TiO_5[] units are close to ideal, as expected based on the first rule. Since these surfaces are reduced, it is reasonable to assume that the average oxidation state of Ti is also reduced. As such, the presence of TiO_3 is plausible because of the highly-reduced nature of these surfaces. Additionally, TiO_3 units only occur in situations with very low excess TiO_x, consistent with the other surfaces analyzed. Coordination of TiO_3 should obey Pauling's rules as well, adopting the most ideal polyhedron geometry possible.

Pauling's third and fourth rules are obeyed; TiO_x units are organized such that face sharing does not occur and edge-sharing is also minimized. The TiO_3 units also follow this rule, and they only share corners with other TiO_x. This behavior is as expected from their extremely low coordination and high valence. While not enough structures have been solved to conduct the same type of analysis done on the $SrTiO_3$ surfaces, the available information provides clues for solving additional $BaTiO_3$ reconstructions.

These structures also illustrate another use of Pauling's rules – to raise questions with structures which appear to deviate from what is normal. For instance, both contain surface titanyl group with a Ti═O double bond. This is unusual, as it yields a “naked” polyhedral apex. In addition, the proposed three-fold titanium sites are not what one would expect based upon established bulk inorganic chemistry.

4.6. $LaAlO_3$ (110)

Moving beyond perovskites that contain titanium, the only other oxide material which has multiple reconstructions both reported and solved in a quantitative manner is $LaAlO_3$ (110).

$LaAlO_3$ has been of interest in the oxide community since the discovery of at 2-dimensional electron gas at the $LaAlO_3$/$SrTiO_3$ (100) interface [1]. Unlike $SrTiO_3$, where the valence of the two cations is viewed as +2/+4 (Sr/Ti), in $LaAlO_3$ it is +3/+3 (La/Al). This leads to a polar surface for the $LaAlO_3$ (100) termination. The (110) termination can also be thought of as an alternate stacking of $(LaAlO)^{4+}$ and $(O_2)^{4-}$ layers, possessing a macroscopic electrostatic dipole similar to that of $SrTiO_3$ (110). The parallels to the $SrTiO_3$ surface do not end there-the two reconstructions reported on the $LaAlO_3$ (110) surface, (2 × 1) [117] and (3 × 1) [88], have many similarities to the (n × 1) reconstructions on the $SrTiO_3$ (110) surface [77,78]. For $LaAlO_3$, the solved reconstructions can be described as Al_2O_3-rich (as opposed to TiO_2-rich), and are all neutral in terms of formal charge. Ideally, they conform to the formula nLaAlO$_3$•mAl$_2$O$_3$, although the (3 × 1) has additional adsorbed hydrogen (i.e. −OH groups). The structures of the (2 × 1) and (3 × 1) are shown in Fig. 13.

The reconstructions shown in Fig. 13 are very similar to those on the $SrTiO_3$ (110) surface with similar polyhedral elements, AlO_4 and AlO_5[] present. This agrees with Pauling's fifth rule. Additionally, these units occur at similar positions with respect to the underlying bulk layers when compared to the TiO_4 on the $SrTiO_3$ (110) surface. These AlO_4 and AlO_5[] are as close as possible to ideal polyhedra for these coordination numbers, in accordance with Pauling's first rule. Deviations from ideal polyhedron shapes are due more to cation repulsion and close packing of polyhedra than any other factor, as expected from Pauling's first rule. The reconstructions shown here also conform to Pauling's third and fourth rules. Face and edge sharing between AlO_x units are minimized while still conforming to the experimental unit cell size and lack of formal charge requirements.

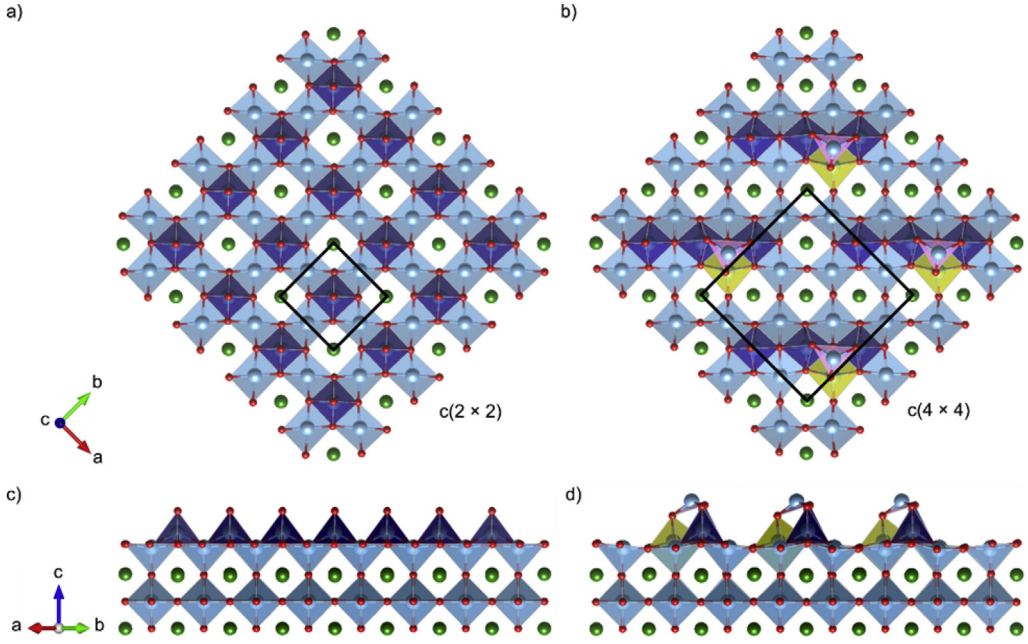

Fig. 12. Atomic structure of reconstructions on $BaTiO_3$ (100) surface showing c(2 × 2) viewed down perpendicular axes in (a) and (c) and c(4 × 4) viewed down the same perpendicular axes in (b) and (d). TiO_6 units are light blue, surface TiO_6 are yellow, TiO_5[] are navy blue, and TiO_3 are pink. Ba atoms are dark green, Ti are blue, and oxygen are red. (For interpretation of the references to color in this figure legend, the reader is referred to the Web version of this article.)

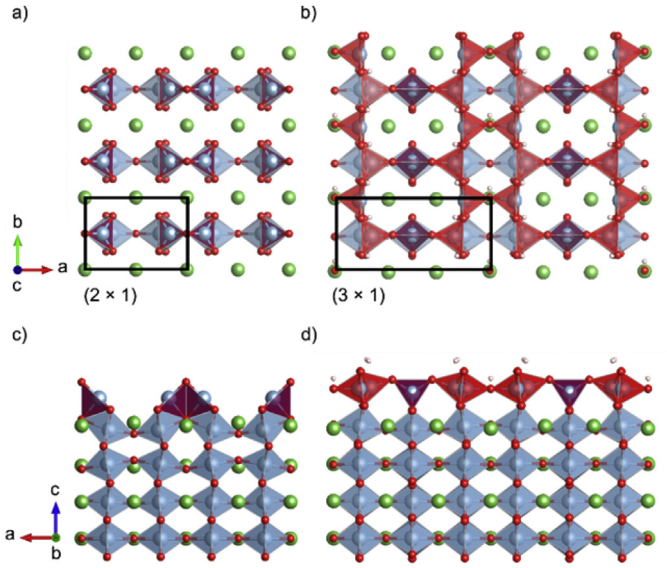

Fig. 13. Atomic structure of the solved reconstructions on $LaAlO_3$ (110) surface showing (2 × 1) in viewed down the c-axis in (a) and viewed down the b-axis in (c). Atomic structure of the solved (3 × 1) reconstruction viewed down the c-axis in (b) and the b-axis in (d). AlO_6 units are light blue, and two different orientations of AlO_4 are red and purple respectively. La atoms are green, Al are blue, and oxygen are red. (For interpretation of the references to color in this figure legend, the reader is referred to the Web version of this article.)

The formula to describe charge neutral reconstructions is different for this surface than $SrTiO_3$ (110) in B-site cation and oxygen content: i.e. $n LaAlO_3 \bullet m Al_2O_3$ vs. $n SrTiO_3 \bullet m TiO_2$. As such, it may seem surprising that these reconstructions have such features. However, the fact that the same types of structural units appear on both oxide surfaces indicates that they could be codified in a very similar manner. This further reinforces the idea that Pauling's rules provide a robust framework for oxide surfaces.

5. Discussion

By using the large number of reconstructions solved on the (100), (110), and (111) orientations of $SrTiO_3$ and a few other materials as examples, the application of Pauling's rules to oxide surfaces has been demonstrated. Although these surfaces have disparate properties, the fundamental features and structural motifs found on them are remarkably similar. All orientations of $SrTiO_3$ exhibit families of related reconstructions based on a Ti-rich surface that most often consists of a bulk-like Ti-atom layer with additional TiO_x polyhedra sitting on top of it, creating the various electron density features often probed via STM, SXRD, or TED. In all cases discussed, these reconstructions can be represented by tilings of only a few different structural units in an Ising or Potts model, with polyhedra of TiO_6, TiO_5[], and TiO_4 possessing near-ideal bond Ti—O bond lengths and angles occurring consistently across different orientations. In addition, reconstructions on these surfaces follow Pauling's other rules in their specific arrangements-reducing the number of face and edge sharing polyhedral units further as the coordination number of a high valence cation, in this case Ti^{4+}, decreases.

The surface of $SrTiO_3$ is currently the largest database where all atomic positions of both experimentally observed and alternative candidates are freely available. As discussed in the text, there are a few other cases where sufficient information is freely available, for a few $LaAlO_3$ and $BaTiO_3$ surfaces. There are also other cases where a fair amount is already known such as TiO_2 surfaces, MgO and NiO surfaces with water as well as reconstructed Al_2O_3 on NiAl (110) and $NiWO_4$ [118–131]. There have also been surface structures solved or proposed on $LiNbO_3$ [89], $PbTiO_3$ [90], and likely other perovskite surfaces. However, none of these data sets contain a number of structures large enough to draw conclusions regarding their structural units.

To our knowledge all oxide surfaces (and others if we include organics or elemental semiconductors) where there is definitive data follow Pauling's rules; with simpler surfaces such as the hydroxylated rock-salt (111) surfaces the polyhedra are quite simple and are just Ising model structures, whereas TiO_2 surfaces are universally based around TiO_4 tetrahedra, or TiO_5[] and TiO_6 octahedra. Unfortunately it is still too common (in our opinion) for theoretical or experimental surface structures to be published with inadequate disclosure of atomic positions, which makes a detailed analysis problematic. In addition, in some cases very thin surface slabs are used, and/or some of the atomic positions are fixed. As pointed out some time ago the BVS sums converge relatively slowly with slab thickness so this can lead to artifacts [100].

While it is not impossible that there are rare cases where Pauling's rules are not obeyed, based upon our analysis of the available literature we know of none where they are violated. The concepts of electrostatic repulsion and its balance with electronegativity as well as the influence of bonding orbitals are universal and effectively at the heart of the BVS model as well as Pauling's rules in general, giving them broad applicability. This has been demonstrated beyond reasonable doubt for bulk materials; surfaces are really not that different.

With a set of rules established based on Pauling's rules, the task of generating plausible solutions for additional reconstructions on this material is significantly simplified. It is even possible to generate hypothetical structural solutions for surface reconstructions where little data is present or of arbitrary unit cell dimensions. To do this, the Ising or Potts models serve as a starting point for generating reconstructions on the various surfaces. In this way, Pauling's rules can be combined with simple algorithms to generate every possible solution for a given unit cell size. This has been demonstrated for the $SrTiO_3$ (100) surface with the prediction of new, low energy surface structures [132]. While some surfaces of $SrTiO_3$ are more complex than others, and the number of possible reconstructions quickly becomes very large as the unit cell size increases, this strategy could still be employed in cases where little information is available regarding a given structure. The combination of these rules with algorithms designed to generate permutations of possible structures offers a truly predictive capability for oxide surfaces. Even in cases of large unit cells, Pauling's rules can be used to generate realistic hypothetical structures or evaluate the likelihood of a given proposed structure. Unfortunately these rules do not provide any guidance regarding the ratio of cations present (i.e. the n and m values in $n SrTiO_3 \bullet m TiO_2$), so it is at-present necessary to generate all possible solutions for a given unit cell size unless additional experimental information is available. When combined with additional data including symmetry and relative surface composition from STM, SXRD, TED, or other methods, this can significantly reduce the number of candidate structures to evaluate using *ab initio* methods like DFT. Along with the simple BVS calculation method, these rules provide an alternative initial evaluation method with essentially negligible computational cost. This results in an overall reduction in computation time and expense as fewer structures need to be considered and reconstructions with otherwise prohibitively large unit cells can be treated in a systematic manner.

Once a set of hypothetical structures are generated using an appropriate algorithm, these structures can be initially compared using BVS model calculations to eliminate structures that deviate

greatly from the expected BVS or compare unfavorably to other structures with the same unit cell size [100]. This can serve as a quick screening method before moving on to more-expensive calculations. The remaining hypotheses serve as starting points for DFT relaxations. Relaxation of the structures can then be performed to compare the surface energies of different structures and determine which is lowest in energy or matches most closely with available experimental data. When a structure generated through the application of Pauling's rules is relaxed the atoms will shift some from their original positions. Whether a given TiO_x polyhedra is better-described in the end as TiO_4 with long bonds to other oxygen atoms, TiO_5[] or TiO_6 is relevant, but not critical since the overall number of atoms is constant.

Two additional oxide surfaces, $BaTiO_3$ (100) and $LaAlO_3$ (110) are also shown to conform to Pauling's rules, although the bonding in the proposed $BaTiO_3$ structures is surprising. This shows that Pauling's rules are applicable to oxide perovskites of different cations and oxidations states. The cases of reduced and hydrated surfaces were briefly mentioned in these datasets and the majority of the solved reconstructions on $SrTiO_3$ surfaces are air-stable at room temperature (not only under vacuum). As these cases resulted in only small deviations from the expectations laid out by Pauling's rules, they do not present a significant deviation from this framework. This implies that any surface that is not currently undergoing a chemical reaction where its stoichiometry changes can be analyzed with these methods. When using this approach to analyze an oxide surface where little is known, either oxides of similar bulk structure or atomic species can be used as a starting point-the polyhedral units of the cation-anion building blocks can be inferred from bulk inorganic chemistry. The paucity of data regarding solved reconstructions for other perovskite oxide surfaces is a perfect test bed that we will leave to the future.

The analysis presented here focused mainly on reconstructions at surfaces, however there is evidence in some cases that a disordered surface, or one where only local-range order is maintained is the lowest-energy solution. This was reported as the case on the $SrTiO_3$ (111) surface where a number of very small unit cell reconstructions had similar surface energy leading to the presence of a 2-D network glass structure having features of local ordering but globally representing a mixture of more than one surface [11,20,101]. It has also been reported on the CeO_2 (100) surface where it was argued that disorder can provide a mechanism for surface stabilization [133]. In these cases the predictive power of Pauling's rules becomes limited from an algorithmic standpoint as cases with no specific unit cell size or very little symmetry are inherently more difficult to calculate. These are not cases where Pauling's rules break down, as the fundamental cation-anion polyhedral units are still the same types of building blocks present in any reconstruction. While there may be no long-range order, local arrangements can still be assessed and compared to each other using these rules or generated according to them. Essentially, Pauling's rules still provide insight into what the local arrangement of atoms is most likely to be even in surfaces with little order.

The reconstructions presented here are thermodynamically stable structures, introducing the question of whether surfaces formed under conditions where kinetics dominate (i.e. film growth) also adhere to Pauling's rules. The available evidence says, yes; however, there have not been enough studies where both the substrate surface and resultant film surface structure are considered. Those studies which the authors are currently aware involve deposition methods including molecular beam epitaxy, reactive (or hybrid) molecular beam epitaxy, and pulsed laser deposition. These have found reconstructions to be a persistent feature in homoepitaxial $SrTiO_3$ growth for multiple orientations. This is evidenced by the presence of the same types of reconstructions in thin films as on the "bare" surfaces. Persistence of the $(\sqrt{13} \times \sqrt{13})R33.7^\circ$ (RT13) reconstruction on a $SrTiO_3$ (100) substrate was observed via STM after the initial stages of PLD thin film growth. In this case, the reconstruction migrated to the surface [134]. Sub-monolayer $LaAlO_3$ (100) growth on $SrTiO_3$ (100) was conducted where the substrate's RT13 reconstruction was observed to migrate, forming a thin TiO_2 layer at the surface [135]. A study of homoepitaxial growth on $SrTiO_3$ (100) considered surfaces with a (2×2) or the $c(6 \times 2)$ reconstruction and found that films grown on these surfaces had different morphologies [136]. Growth of $La_{0.7}Ca_{0.3}MnO_3$ on $SrTiO_3$ (100) RT13 surfaces indicated that the initial excess Ti on the surface led to films displaying a surface structure of the same periodicity even up to a thickness of 50 unit cells [137]. During the process of growth, subtle variation of Sr:Ti cation ratio produces different, previously-observed, reconstructions in films grown by hybrid molecular beam epitaxy on $SrTiO_3$ (100) and (110) [19,78]. The appearance of reconstructions, and the A:B cation ratio they imply, is reliable and repeatable enough that they have even been successfully used for *in situ* feedback to control $SrTiO_3$ film stoichiometry during deposition [116]. This indicates that changing the number of fundamental TiO_x units (by varying the A:B stoichiometry) causes a surface to re-organize itself to obey Pauling's rules.

In summary, all the available evidence points towards Pauling's rules being applicable to perovskite surfaces, where there is currently a large enough database of well-solved structures. We see no reason why the rules should be limited to perovskites, and they should be generally applicable to other oxides. Indeed, there is no reason to limit their use to oxides, and in fact they have been implicitly used for silicon and related III–IV materials where similar ideas are common. These are Pauling's rules and just different types of coordination chemistry.

Surface structures that disobey Pauling's rules must be treated with caution. They might be rare exceptions, or just incorrect interpretations; this we leave to the future.

Acknowledgements

We would like to thank in particular Professors Kenneth Poeppelmeier and James Rondinelli for numerous discussions as these concepts evolved over the years. This work used the Extreme Science and Engineering Discovery Environment (XSEDE), which is supported by National Science Foundation grant number ACI-1548562. Specifically, it used the Bridges system, which is supported by NSF award number ACI-1445606, at the Pittsburgh Supercomputing Center (PSC) through allocation DMR160023P [138,139]. T.K.A. and D.D.F were supported by the U.S. Department of Energy, Office of Science, Office of Basic Energy Sciences, Materials Sciences and Engineering Division. LDM acknowledges support by both the U.S. Department of Energy, Office of Science, Basic Energy Sciences, under Award # DE-FG02-01ER45945 and the National Science Foundation (NSF) under grant number DMR-1507101 for the evolution of these ideas over many years. Many of the structures described herein were analyzed using the all-electron augmented plane wave + local orbitals WIEN2K code [140].

References

[1] A. Ohtomo, H.Y. Hwang, A high-mobility electron gas at the $LaAlO_3/SrTiO_3$ heterointerface, Nature 427 (2004) 423–426.
[2] S. Tsui, A. Baikalov, J. Cmaidalka, Y.Y. Sun, Y.Q. Wang, Y.Y. Xue, C.W. Chu, L. Chen, A.J. Jacobson, Field-induced resistive switching in metal-oxide interfaces, Appl. Phys. Lett. 85 (2004) 317–319.
[3] J. Mannhart, D.G. Schlom, Oxide interfaces- an opportunity for electronics, Science 327 (2010) 1607–1611.
[4] J. Suntivich, H.A. Gasteiger, N. Yabuuchi, H. Nakanishi, J.B. Goodenough, Y. Shao-Horn, Design principles for oxygen-reduction activity on perovskite oxide catalysts for fuel cells and metal-air batteries, Nat. Chem. 3 (2011) 546.

[5] Y. Lin, J. Wen, L. Hu, R.M. Kennedy, P.C. Stair, K.R. Poeppelmeier, L. Marks, Synthesis-dependent atomic surface structures of oxide nanoparticles, Phys. Rev. Lett. 111 (2013) 156101.

[6] Z. Feng, W.T. Hong, D.D. Fong, Y.-L. Lee, Y. Yacoby, D. Morgan, Y. Shao-Horn, Catalytic activity and stability of oxides: the role of near-surface atomic structures and compositions, Acc. Chem. Res. 49 (2016) 966–973.

[7] J.T. Mefford, R. Xi, M.A. Artem, G.H. William, D. Sheng, M.K. Alexie, P.J. Keith, J.S. Keith, Water electrolysis on $La_{1-x}Sr_xCoO_{3-\delta}$ perovskite electrocatalysts, Nat. Commun. 7 (2016) 11053.

[8] M. O'Sullivan, J. Hadermann, M.S. Dyer, S. Turner, J. Alaria, T.D. Manning, A.M. Abakumov, J.B. Claridge, M.J. Rosseinsky, Interface control by chemical and dimensional matching in an oxide heterostructure, Nat. Chem. 8 (2016) 347–353.

[9] A.N. Chiaramonti, C.H. Lanier, L.D. Marks, P.C. Stair, Time, temperature, and oxygen partial pressure-dependent surface reconstructions on $SrTiO_3$ (111): a systematic study of oxygen-rich conditions, Surf. Sci. 602 (2008) 3018–3025.

[10] B.C. Russell, M.R. Castell, Surface of sputtered and annealed polar $SrTiO_3$ (111): TiO_x-Rich ($n \times n$) reconstructions, J. Phys. Chem. C 112 (2008) 6538–6545.

[11] L.D. Marks, A.N. Chiaramonti, S.U. Rahman, M.R. Castell, Transition from order to configurational disorder for surface reconstructions on $SrTiO_3$ (111), Phys. Rev. Lett. 114 (2015) 226101.

[12] R.J. Hamers, R. Tromp, J.E. Demuth, Surface electronic structure of Si (111)-(7× 7) resolved in real space, Phys. Rev. Lett. 56 (1986) 1972–1977.

[13] K.D. Brommer, M. Needels, B. Larson, J. Joannopoulos, Ab initio theory of the Si (111)-(7× 7) surface reconstruction: a challenge for massively parallel computation, Phys. Rev. Lett. 68 (1992) 1355–1359.

[14] F.J. Giessibl, Atomic resolution of the silicon (111)-(7x7) surface by atomic force microscopy, Science 267 (1995) 68–71.

[15] N. Erdman, K.R. Poeppelmeier, M. Asta, O. Warschkow, D.E. Ellis, L.D. Marks, The structure and chemistry of the TiO_2-rich surface of $SrTiO_3$ (001), Nature 419 (2002) 55–58.

[16] S. Gerhold, Z. Wang, M. Schmid, U. Diebold, Stoichiometry-driven switching between surface reconstructions on $SrTiO_3$ (001), Surf. Sci. 621 (2014) L1–L4.

[17] L. Hu, C. Wang, R.M. Kennedy, L.D. Marks, K.R. Poeppelmeier, The role of oleic acid: from synthesis to assembly of perovskite nanocuboid two-dimensional arrays, Inorg. Chem. 54 (2014) 740–745.

[18] B. Jalan, R. Engel-Herbert, N.J. Wright, S. Stemmer, Growth of high-quality $SrTiO_3$ films using a hybrid molecular beam epitaxy approach, J. Vac. Sci. Technol., A 27 (2009) 461–464.

[19] A.P. Kajdos, S. Stemmer, Surface reconstructions in molecular beam epitaxy of $SrTiO_3$, Appl. Phys. Lett. 105 (2014) 191901.

[20] D.M. Kienzle, A.E. Becerra-Toledo, L.D. Marks, Vacant-site octahedral tilings on $SrTiO_3$ (001), the ($\sqrt{13} \times \sqrt{13}$)R33.7° surface, and related structures, Phys. Rev. Lett. 106 (2011) 176102.

[21] F. Silly, D.T. Newell, M.R. Castell, $SrTiO_3$ (0 0 1) reconstructions: the (2 × 2) to c (4 × 4) transition, Surf. Sci. 600 (2006) 219–223.

[22] J. He, A. Borisevich, S.V. Kalinin, S.J. Pennycook, S.T. Pantelides, Control of octahedral tilts and magnetic properties of perovskite oxide heterostructures by substrate symmetry, Phys. Rev. Lett. 105 (2010) 227203.

[23] R. Aso, D. Kan, Y. Shimakawa, H. Kurata, Atomic level observation of octahedral distortions at the perovskite oxide heterointerface, Sci. Rep. 3 (2013) 2214.

[24] F. Sánchez, C. Ocal, J. Fontcuberta, Tailored surfaces of perovskite oxide substrates for conducted growth of thin films, Chem. Soc. Rev. 43 (2014) 2272–2285.

[25] D.G. Schlom, L.-Q. Chen, C.J. Fennie, V. Gopalan, D.A. Muller, X. Pan, R. Ramesh, R. Uecker, Elastic strain engineering of ferroic oxides, MRS Bull. 39 (2014) 118–130.

[26] M. Corso, W. Auwarter, M. Muntwiler, A. Tamai, T. Greber, J. Osterwalder, Boron nitride nanomesh, Science 303 (2004) 217–220.

[27] F. Silly, M.R. Castell, Selecting the shape of supported metal nanocrystals: Pd huts, hexagons, or pyramids on SrTiO3(001), Phys. Rev. Lett. 94 (2005), 046103.

[28] F. Silly, M.R. Castell, Growth of Ag icosahedral nanocrystals on a $SrTiO_3$(001) support, Appl. Phys. Lett. 87 (2005) 213107.

[29] F. Silly, M.R. Castell, Fe nanocrystal growth on $SrTiO_3$(001), Appl. Phys. Lett. 87 (2005), 063106.

[30] F. Silly, M.R. Castell, Self-assembled supported Co nanocrystals: the adhesion energy of face-centered-cubic Co on SrTiO3(001)-(2x2), Appl. Phys. Lett. 87 (2005), 053106.

[31] M. Schmid, G. Kresse, A. Buchsbaum, E. Napetschnig, S. Gritschneder, M. Reichling, P. Varga, Nanotemplate with holes: ultrathin alumina on Ni_3Al(111), Phys. Rev. Lett. 99 (2007) 196104.

[32] K. Ait-Mansour, A. Buchsbaum, P. Ruffieux, M. Schmid, P. Groning, P. Varga, R. Fasel, O. Groning, Fabrication of a well-ordered nanohole array stable at room temperature, Nano Lett. 8 (2008) 2035–2040.

[33] C. Becker, K. Wandelt, Surfaces: two-dimensional templates, in: P. Broekmann, K.H. Dotz, C.A. Schalley (Eds.), Templates in Chem, vol. III, Springer-Verlag Berlin, Berlin, 2009, pp. 45–86.

[34] Z.Q. Zhang, J.G. Feng, Z.M. Wang, F. Yang, Q.L. Guo, J.D. Guo, Guided growth of Ag nanoparticles on $SrTiO_3$ (110) surface, J. Chem. Phys. 135 (2011) 144702.

[35] J.G. Mavroides, J.A. Kafalas, D.F. Kolesar, Photoelectrolysis of water in cells with $SrTiO_3$ anodes, Appl. Phys. Lett. 28 (1976) 241–243.

[36] D. Cappus, M. Hassel, E. Neuhaus, M. Heber, F. Rohr, H.J. Freund, Polar surfaces of oxides – Reactivity and reconstruction, Surf. Sci. 337 (1995) 268–277.

[37] U. Diebold, The surface science of titanium dioxide, Surf. Sci. Rep. 48 (2003) 53–229.

[38] G. Centi, S. Perathoner, Catalysis by layered materials: a review, Microporous Mesoporous Mater. 107 (2008) 3–15.

[39] T.K. Townsend, N.D. Browning, F.E. Osterloh, Nanoscale strontium titanate photocatalysts for overall water splitting, ACS Nano 6 (2012) 7420–7426.

[40] Y. Wang, H.J. Sun, S.J. Tan, H. Feng, Z.W. Cheng, J. Zhao, A.D. Zhao, B. Wang, Y. Luo, J.L. Yang, J.G. Hou, Role of point defects on the reactivity of reconstructed anatase titanium dioxide (001) surface, Nat. Commun. 4 (2013) 2214.

[41] N. Reyren, S. Thiel, A.D. Caviglia, L.F. Kourkoutis, G. Hammerl, C. Richter, C.W. Schneider, T. Kopp, A.S. Rüetschi, D. Jaccard, M. Gabay, D.A. Muller, J.M. Triscone, J. Mannhart, Superconducting interfaces between insulating oxides, Science 317 (2007) 1196–1199.

[42] S. Gariglio, J.-M. Triscone, Oxide interface superconductivity, Compt. Rendus Phys. 12 (2011) 591–599.

[43] H.Y. Hwang, Y. Iwasa, M. Kawasaki, B. Keimer, N. Nagaosa, Y. Tokura, Emergent phenomena at oxide interfaces, Nat. Mater. 11 (2012) 103–113.

[44] N.J.C. Ingle, A. Yuskauskas, R. Wicks, M. Paul, S. Leung, The structural analysis possibilities of reflection high energy electron diffraction, J. Phys. D Appl. Phys. 43 (2010) 133001.

[45] E.A. Soares, C.M.C. de Castilho, V.E. de Carvalho, Advances on surface structural determination by LEED, J. Phys. Condens. Matter 23 (2011) 303001.

[46] H. Onishi, Y. Iwasawa, Reconstruction of TiO_2 (110) surface: STM study with atomic-scale resolution, Surf. Sci. 313 (1994) L783–L789.

[47] M.R. Castell, Scanning tunneling microscopy of reconstructions on the $SrTiO_3$(001) surface, Surf. Sci. 505 (2002) 1–13.

[48] B.C. Russell, M.R. Castell, Reconstructions on the polar $SrTiO_3$ (110) surface: analysis using STM, LEED, and AES, Phys. Rev. B Condens. Matter 77 (2008) 245414.

[49] J. Tersoff, D.R. Hamann, Theory of the scanning tunneling microscope, Phys. Rev. B Condens. Matter 31 (1985) 805–813.

[50] A.E. Becerra-Toledo, M.S.J. Marshall, M.R. Castell, L.D. Marks, c(4 × 2) and related structural units on the $SrTiO_3$ (001) surface: scanning tunneling microscopy, density functional theory, and atomic structure, J. Chem. Phys. 136 (2012) 214701.

[51] D.M. Kienzle, L.D. Marks, Surface transmission electron diffraction for $SrTiO_3$ surfaces, CrystEngComm 14 (2012) 7833–7839.

[52] I. Robinson, D. Tweet, Surface X-Ray diffraction, Rep. Prog. Phys. 55 (1992) 599–651.

[53] R. Herger, P.R. Willmott, O. Bunk, C.M. Schlepütz, B.D. Patterson, B. Delley, V.L. Shneerson, P.F. Lyman, D.K. Saldin, Surface structure of $SrTiO_3$ (001), Phys. Rev. B Condens. Matter 76 (2007) 195435.

[54] M.M. Woolfson, H.-f. Fan, Physical and Non-physical Methods of Solving Crystal Structures, Cambridge University Press, Cambridge, New York, 1995.

[55] L.D. Marks, W. Sinkler, E. Landree, A feasible set approach to the crystallographic phase problem, Acta Crystallogr. Sect. A 55 (1999) 601–612.

[56] H.D. Megaw, Crystal structure of double oxides of the perovskite type, Proc. Phys. Soc. 58 (1946) 133–152.

[57] B. Cord, R. Courths, Electronic study of $SrTiO_3$ (001) surfaces by photoemission, Surf. Sci. 162 (1985). A572-A572.

[58] J.E.T. Andersen, P.J. Møller, Impurity-induced 900° C (2 × 2) surface reconstruction of $SrTiO_3$ (100), Appl. Phys. Lett. 56 (1990) 1847–1849.

[59] M. Naito, H. Sato, Reflection high-energy electron diffraction study on the $SrTiO_3$ surface structure, Physica C 229 (1994) 1–11.

[60] H. Tanaka, T. Matsumoto, T. Kawai, S. Kawai, Interaction of oxygen vacancies with O_2 on a reduced $SrTiO_3$ (100) $\sqrt{5} \times \sqrt{5}$-R26.6° surface observed by STM, Surf. Sci. 318 (1994) 29–38.

[61] H. Bando, Y. Aiura, Y. Haruyama, T. Shimizu, Y. Nishihara, Structure and electronic states on reduced $SrTiO_3$(110) surface observed by scanning-tunneling-microscopy and spectroscopy, J. Vac. Sci. Technol. B 13 (1995) 1150–1154.

[62] Q.D. Jiang, J. Zegenhagen, $SrTiO_3$ (001) surfaces and growth of ultra-thin $GdBa_2Cu_3O_{7-x}$ films studied by LEED/AES and UHV-STM, Surf. Sci. 338 (1995) L882–L888.

[63] J. Brunen, J. Zegenhagen, Investigation of the $SrTiO_3$ (110) surface by means of LEED, scanning tunneling microscopy and Auger spectroscopy, Surf. Sci. 389 (1997) 349–365.

[64] Y. Haruyama, Y. Aiura, H. Bando, Y. Nishihara, H. Kato, Annealing temperature dependence on the electronic structure of the reduced $SrTiO_3$ (111) surface, J. Electron. Spectrosc. Relat. Phenom. 88 (1998) 695–699.

[65] S. Sekiguchi, M. Fujimoto, M. Nomura, S.-B. Cho, J. Tanaka, T. Nishihara, M.-G. Kang, H.-H. Park, Atomic force microscopic observation of $SrTiO_3$ polar surface, Solid State Ionics 108 (1998) 73–79.

[66] Q.D. Jiang, J. Zegenhagen, c(6 × 2) and c(4 × 2) reconstruction of $SrTiO_3$ (001), Surf. Sci. 425 (1999) 343–354.

[67] P.J. Møller, S.A. Komolov, E.F. Lazneva, Selective growth of a MgO (100)-c(2 × 2) superstructure on a $SrTiO_3$ (100)-(2 × 2) substrate, Surf. Sci. 425 (1999) 15–21.

[68] M.S. Martin-Gonzalez, M.H. Aguirre, E. Moran, M.A. Alario-Franco, V. Perez-Dieste, J. Avila, M.C. Asensio, In situ reduction of (100) $SrTiO_3$, Solid State Sci. 2 (2000) 519–524.

[69] T. Kubo, H. Nozoye, Surface structure of $SrTiO_3$ (100)-($\sqrt{5} \times \sqrt{5}$)R26.6°, Phys. Rev. Lett. 86 (2001) 1801–1804.
[70] M.R. Castell, Nanostructures on the $SrTiO_3$(001) surface studied by STM, Surf. Sci. 516 (2002) 33–42.
[71] N. Erdman, O. Warschkow, M. Asta, K.R. Poeppelmeier, D.E. Ellis, L.D. Marks, Surface structures of $SrTiO_3$ (001): a TiO_2-rich reconstruction with a c(4 × 2) unit cell, J. Am. Chem. Soc. 125 (2003) 10050–10056.
[72] T. Kubo, H. Nozoye, Surface structure of $SrTiO_3$ (100), Surf. Sci. 542 (2003) 177–191.
[73] A. Gomann, K. Gomann, M. Frerichs, V. Kempter, G. Borchardt, W. Maus-Friedrichs, Electronic structure and topography of annealed $SrTiO_3$ (111) surfaces studied with MIES and STM, Appl. Surf. Sci. 252 (2005) 196–199.
[74] C. Lanier, A. van de Walle, N. Erdman, E. Landree, O. Warschkow, A. Kazimirov, K.R. Poeppelmeier, J. Zegenhagen, M. Asta, L.D. Marks, Atomic-scale structure of the $SrTiO_3$ (001)-c(6 × 2) reconstruction: experiments and first-principles calculations, Phys. Rev. B Condens. Matter 76 (2007), 045421.
[75] B.C. Russell, M.R. Castell, ($\sqrt{13} \times \sqrt{13}$)R13.9° and ($\sqrt{7} \times \sqrt{7}$)R19.1° reconstructions of the polar $SrTiO_3$ (111) surface, Phys. Rev. B Condens. Matter 75 (2007) 155433.
[76] L.D. Marks, A.N. Chiaramonti, F. Tran, P. Blaha, The small unit cell reconstructions of $SrTiO_3$ (111), Surf. Sci. 603 (2009) 2179–2187.
[77] J.A. Enterkin, A.K. Subramanian, B.C. Russell, M.R. Castell, K.R. Poeppelmeier, L.D. Marks, A homologous series of structures on the surface of $SrTiO_3$ (110), Nat. Mater. 9 (2010) 245–248.
[78] F. Li, Z. Wang, S. Meng, Y. Sun, J. Yang, Q. Guo, J. Guo, Reversible transition between thermodynamically stable phases with low density of oxygen vacancies on the $SrTiO_3$ (110) surface, Phys. Rev. Lett. 107 (2011), 036103.
[79] Y. Lin, A.E. Becerra-Toledo, F. Silly, K.R. Poeppelmeier, M.R. Castell, L.D. Marks, The (2 × 2) reconstructions on the $SrTiO_3$ (001) surface: a combined scanning tunneling microscopy and density functional theory study, Surf. Sci. 605 (2011) L51–L55.
[80] J. Ciston, H.G. Brown, A.J. D'Alfonso, P. Koirala, C. Ophus, Y. Lin, Y. Suzuki, H. Inada, Y. Zhu, L.J. Allen, L.D. Marks, Surface determination through atomically resolved secondary-electron imaging, Nat. Commun. 6 (2015) 7358.
[81] Z. Wang, A. Loon, A. Subramanian, S. Gerhold, E. McDermott, J.A. Enterkin, M. Hieckel, B.C. Russell, R.J. Green, A. Moewes, J. Guo, P. Blaha, M.R. Castell, U. Diebold, L.D. Marks, Transition from reconstruction toward thin film on the (110) surface of strontium titanate, Nano Lett. 16 (2016) 2407–2412.
[82] T.K. Andersen, S. Wang, M.R. Castell, D.D. Fong, L.D. Marks, Single-layer TiO_x reconstructions on $SrTiO_3$ (111):($\sqrt{7} \times \sqrt{7}$) R19. 1°,($\sqrt{13} \times \sqrt{13}$) R13. 9°, and related structures, Surf. Sci. 675 (2018) 36–41.
[83] A.M. Kolpak, A.M. Rappe, D. Li, R. Shao, D.A. Bonnell, Evolution of the structure and thermodynamic stability of the $BaTiO_3$ (001) surface, Phys. Rev. Lett. 101 (2008), 036102.
[84] J.M.P. Martirez, E.H. Morales, W.A. Saidi, D.A. Bonnell, A.M. Rappe, Atomic and electronic structure of the $BaTiO_3$ (001) ($\sqrt{5} \times \sqrt{5}$)R26.6° surface reconstruction, Phys. Rev. Lett. 109 (2012) 256802.
[85] H.L. Meyerheim, A. Ernst, K. Mohseni, I.V. Maznichenko, S. Ostanin, F. Klimenta, N. Jedrecy, W. Feng, I. Mertig, R. Felici, J. Kirschner, $BaTiO_3$ (001)-(2 × 1): surface structure and spin density, Phys. Rev. Lett. 108 (2012) 215502.
[86] E.H. Morales, D.A. Bonnell, On the relationship between surface reconstructions and step edge stability on BaTiO 3 (001), Surf. Sci. 609 (2013) 62–66.
[87] E.H. Morales, J.M.P. Martirez, W.A. Saidi, A.M. Rappe, D.A. Bonnell, Coexisting surface phases and coherent one-dimensional interfaces on $BaTiO_3$ (001), ACS Nano 8 (2014) 4465–4473.
[88] D.M. Kienzle, P. Koirala, L.D. Marks, Lanthanum aluminate (110) 3 × 1 surface reconstruction, Surf. Sci. 633 (2015) 60–67.
[89] S. Sanna, S. Rode, R. Hölscher, S. Klassen, C. Marutschke, K. Kobayashi, H. Yamada, W. Schmidt, A. Kühnle, Charge compensation by long-period reconstruction in strongly polar lithium niobate surfaces, Phys. Rev. B Condens. Matter 88 (2013) 115422.
[90] A. Munkholm, S.K. Streiffer, M.V.R. Murty, J.A. Eastman, C. Thompson, O. Auciello, L. Thompson, J.F. Moore, G.B. Stephenson, Antiferrodistortive reconstruction of the $PbTiO_3$ (001) surface, Phys. Rev. Lett. 88 (2001), 016101.
[91] M.D. Pashley, Electron counting model and its application to island structures on molecular-beam epitaxy grown GaAs (001) and ZnSe (001), Phys. Rev. B Condens. Matter 40 (1989) 10481–10487.
[92] D. Wolf, Reconstruction of NaCl surfaces from a dipolar solution to the Madelung problem, Phys. Rev. Lett. 68 (1992) 3315.
[93] C. Noguera, Polar oxide surfaces, J. Phys. Condens. Matter 12 (2000) R367–R410.
[94] J. Goniakowski, F. Finocchi, C. Noguera, Polarity of oxide surfaces and nanostructures, Rep. Prog. Phys. 71 (2008), 016501.
[95] Z.L. Wang, A.J. Shapiro, Studies of $LaAlO_3$ (100) surfaces using RHEED and REM. II: $\sqrt{5} \times \sqrt{5}$ surface reconstruction, Surf. Sci. 328 (1995) 159–169.
[96] A.E. Becerra-Toledo, J.A. Enterkin, D.M. Kienzle, L.D. Marks, Water adsorption on $SrTiO_3$(001): II. Water, water, everywhere, Surf. Sci. 606 (2012) 791–802.
[97] A.E. Becerra-Toledo, M.R. Castell, L.D. Marks, Water adsorption on $SrTiO_3$(001): I. Experimental and simulated STM, Surf. Sci. 606 (2012) 762–765.
[98] P. Novák, J. Kuneš, L. Chaput, W.E. Pickett, Exact exchange for correlated electrons, Phys. Status Solidi B 243 (2006) 563–572.
[99] O. Warschkow, M. Asta, N. Erdman, K.R. Poeppelmeier, D.E. Ellis, L.D. Marks, TiO_2-rich reconstructions of $SrTiO_3$ (001): a theoretical study of structural patterns, Surf. Sci. 573 (2004) 446–456.
[100] J.A. Enterkin, A.E. Becerra-Toledo, K.R. Poeppelmeier, L.D. Marks, A chemical approach to understanding oxide surfaces, Surf. Sci. 606 (2012) 344–355.
[101] W.H. Zachariasen, The atomic arrangement in glass, J. Am. Chem. Soc. 54 (1932) 3841–3851.
[102] L. Pauling, The principles determining the structure of complex ionic crystals, J. Am. Chem. Soc. 51 (1929) 1010–1026.
[103] I.D. Brown, D. Altermatt, Bond-valence parameters obtained from a systematic analysis of the inorganic crystal structure database, Acta Crystallogr. Sect. B 41 (1985) 244–247.
[104] I.D. Brown, The Chemical Bond in Inorganic Chemistry: the Bond Valence Model, Oxford University Press, Oxford; New York, 2002.
[105] I.D. Brown, Recent developments in the methods and applications of the bond valence model, Chem. Rev. 109 (2009) 6858–6919.
[106] J.A. Enterkin, A.E. Becerra-Toledo, K.R. Poeppelmeier, L.D. Marks, A chemical approach to understanding oxide surfaces, Surf. Sci. 606 (2012) 344–355.
[107] R.D. Shannon, Revised effective ionic radii and systematic studies of interatomic distances in halides and chalcogenides, Acta Crystallogr. Sect. A 32 (1976) 751–767.
[108] K. Binder, D.P. Landau, Square lattice gases with 2-body and 3-body interactions - a model for the adsorption of hydrogen on Pd(100), Surf. Sci. 108 (1981) 503–525.
[109] M.W. Conner, C. Ebner, Solid physically adsorbed films: a Potts lattice-gas-model study, Phys. Rev. B Condens. Matter 36 (1987) 3683–3692.
[110] C.S. Jayanthi, Surface melting in a Potts lattice-gas model, Phys. Rev. B Condens. Matter 44 (1991) 427–430.
[111] M.A. Zaluskakotur, The kinetic Potts-model in the description of surface dynamics, Surf. Sci. 265 (1992) 196–208.
[112] C. Dobrovolny, L. Laanait, J. Ruiz, Surface transitions of the semi-infinite Potts model II: the low bulk temperature regime, J. Stat. Phys. 116 (2004) 1405–1434.
[113] C. Dobrovolny, L. Laanait, J. Ruiz, Surface transitions of the semi-infinite Potts model I: the high bulk temperature regime, J. Stat. Phys. 114 (2004) 1269–1302.
[114] M.S.J. Marshall, A.E. Becerra-Toledo, L.D. Marks, M.R. Castell, Surface and defect structure of oxide nanowires on $SrTiO_3$, Phys. Rev. Lett. 107 (2011), 086102.
[115] M.S.J. Marshall, A.E. Becerra-Toledo, D.J. Payne, R.G. Egdell, L.D. Marks, M.R. Castell, Structure and composition of linear TiO_x nanostructures on $SrTiO_3$ (001), Phys. Rev. B Condens. Matter 86 (2012) 125416.
[116] Z. Wang, J. Feng, Y. Yang, Y. Yao, L. Gu, F. Yang, Q. Guo, J. Guo, Cation stoichiometry optimization of $SrTiO_3$ (110) thin films with atomic precision in homogeneous molecular beam epitaxy, Appl. Phys. Lett. 100 (2012), 051602.
[117] P. Koirala, E. Steele, A. Gulec, L.D. Marks, Al Rich (111) and (110) Surfaces of $LaAlO_3$, Surf. Sci. 677 (2018) 99–104.
[118] J. Ciston, A. Subramanian, L.D. Marks, Water-driven structural evolution of the polar MgO (111) surface: an integrated experimental and theoretical approach, Phys. Rev. B Condens. Matter 79 (2009), 085421.
[119] F. Finocchi, A. Barbier, J. Jupille, C. Noguera, Stability of rocksalt (111) polar surfaces: beyond the octopole, Phys. Rev. Lett. 92 (2004) 136101.
[120] W.-B. Zhang, B.-Y. Tang, Stability of MgO (111) polar surface: effect of the environment, J. Phys. Chem. C 112 (2008) 3327–3333.
[121] J. Ciston, A. Subramanian, D.M. Kienzle, L.D. Marks, Why the case for clean surfaces does not hold water: structure and morphology of hydroxylated nickel oxide (111), Surf. Sci. 604 (2010) 155–164.
[122] U. Diebold, N. Ruzycki, G.S. Herman, A. Selloni, One step towards bridging the materials gap: surface studies of TiO_2 anatase, Catal. Today 85 (2003) 93–100.
[123] M. Lazzeri, A. Selloni, Stress-driven reconstruction of an oxide surface: the anatase TiO_2 (001)–(1× 4) surface, Phys. Rev. Lett. 87 (2001) 266105.
[124] M. Lazzeri, A. Vittadini, A. Selloni, Structure and energetics of stoichiometric TiO_2 anatase surfaces, Phys. Rev. B Condens. Matter 63 (2001) 155409.
[125] A. Vittadini, A. Selloni, F.P. Rotzinger, M. Grätzel, Structure and energetics of water adsorbed at TiO_2 anatase (101) and (001) surfaces, Phys. Rev. Lett. 81 (1998) 2954.
[126] O. Warschkow, Y. Wang, A. Subramanian, M. Asta, L.D. Marks, Structure and local-equilibrium thermodynamics of the c (2× 2) reconstruction of rutile TiO_2 (100), Phys. Rev. Lett. 100 (2008), 086102.
[127] G. Kresse, M. Schmid, E. Napetschnig, M. Shishkin, L. Köhler, P. Varga, Structure of the ultrathin aluminum oxide film on NiAl (110), Science 308 (2005) 1440–1442.
[128] J.V. Lauritsen, M.C.R. Jensen, K. Venkataramani, B. Hinnemann, S. Helveg, B.S. Clausen, F. Besenbacher, Atomic-Scale structure and stability of the $\sqrt{31} \times \sqrt{31}$R9° surface of Al_2O_3 (0001), Phys. Rev. Lett. 103 (2009), 076103.
[129] T. Nishimura, Y. Hoshino, T. Okazawa, Y. Kido, Structure of an ultrathin aluminum oxide layer grown on a NiAl (110) substrate, Phys. Rev. B Condens. Matter 77 (2008), 073405.
[130] M. Schmid, G. Kresse, A. Buchsbaum, E. Napetschnig, S. Gritschneder, M. Reichling, P. Varga, Nanotemplate with holes: ultrathin alumina on Ni_3Al (111), Phys. Rev. Lett. 99 (2007) 196104.
[131] N. Doudin, S. Pomp, M. Blatnik, R. Resel, M. Vorokhta, J. Goniakowski, C. Noguera, F.P. Netzer, S. Surnev, Epitaxial $NiWO_4$ films on Ni (110):

experimental and theoretical study of surface stability, Surf. Sci. 659 (2017) 20–30.
[132] S. Cook, L.D. Marks, Ab Initio Predictions of TiO_2 Double-layer $SrTiO_3$ (001) Surface Reconstructions, J. Phys. Chem C (2018), https://doi.org/10.1021/acs.jpcc.8b07128.
[133] M. Capdevila-Cortada, N. López, Entropic contributions enhance polarity compensation for CeO_2 (100) surfaces, Nat. Mater. 16 (2017) 328–335.
[134] R. Shimizu, K. Iwaya, T. Ohsawa, S. Shiraki, T. Hasegawa, T. Hashizume, T. Hitosugi, Atomic-scale visualization of initial growth of homoepitaxial $SrTiO_3$ thin film on an atomically ordered substrate, ACS Nano 5 (2011) 7967–7971.
[135] T. Ohsawa, M. Saito, I. Hamada, R. Shimizu, K. Iwaya, S. Shiraki, Z. Wang, Y. Ikuhara, T. Hitosugi, A single-atom-thick TiO_2 nanomesh on an insulating oxide, ACS Nano 9 (2015) 8766–8772.
[136] S.-H. Phark, Y.J. Chang, T. Won Noh, Selective growth of perovskite oxides on $SrTiO_3$ (001) by control of surface reconstructions, Appl. Phys. Lett. 98 (2011) 161908.
[137] R. Shimizu, T. Ohsawa, K. Iwaya, S. Shiraki, T. Hitosugi, Epitaxial growth process of $La_{0.7}Ca_{0.3}MnO_3$ thin films on $SrTiO_3$ (001): thickness-dependent inhomogeneity caused by excess Ti atoms, Cryst. Growth Des. 14 (2014) 1555–1560.
[138] J. Towns, T. Cockerill, M. Dahan, I. Foster, K. Gaither, A. Grimshaw, V. Hazlewood, S. Lathrop, D. Lifka, G.D. Peterson, R. Roskies, J.R. Scott, N. Wilkins-Diehr, XSEDE: accelerating scientific discovery, Comput. Sci. Eng. 16 (2014) 62–74.
[139] N. Nystrom, M. Levine, R. Roskies, J. Scott, Bridges: a Uniquely Flexible HPC Resource for New Communities and Data Analytics, 2015, pp. 1–8.
[140] P. Blaha, K. Schwarz, G.K.H. Madsen, D. Kvasnicka, J. Luitz, R. Laskowsji, F. Tran, L.D. Marks, An Augmented Plane Wave + Local Orbitals Program for Calculating Crystal Properties, Techn. Universitat Wien, Austria, 2018.